

# JGR Space Physics

## RESEARCH ARTICLE

10.1029/2019JA027147

### Key Points:

- A combination of hybrid simulations and particle tracing is applied to study the dynamics of energetic magnetospheric ions near Europa
- Energetic ion dynamics near Europa are strongly affected by the Alfvénic field perturbations near the moon
- In the kiloelectron volt regime, field line draping due to ionospheric mass loading effectively shields Europa's surface against energetic ions

### Correspondence to:

S. Simon,  
sven.simon@eas.gatech.edu

### Citation:

Breer, B. R., Liuzzo, L., Arnold, H., Andersson, P. N., & Simon, S. (2019). Energetic ion dynamics in the perturbed electromagnetic fields near Europa. *Journal of Geophysical Research: Space Physics*, 124, 7592–7613. <https://doi.org/10.1029/2019JA027147>

Received 12 JUL 2019

Accepted 24 AUG 2019

Accepted article online 6 SEP 2019

Published online 17 SEP 2019

## Energetic Ion Dynamics in the Perturbed Electromagnetic Fields Near Europa

Benjamin R. Breer<sup>1</sup> , Lucas Liuzzo<sup>1,2</sup> , Hannes Arnold<sup>1</sup> , Peter N. Andersson<sup>1</sup>, and Sven Simon<sup>1</sup> 

<sup>1</sup>School of Earth and Atmospheric Sciences, Georgia Institute of Technology, Atlanta, GA, USA, <sup>2</sup>Space Sciences Laboratory, University of California, Berkeley, CA, USA

**Abstract** We model the dynamics of energetic magnetospheric ions in the perturbed electromagnetic fields near Jupiter's moon Europa. The inhomogeneities in the fields near Europa are generated by the induced dipole field from the moon's subsurface ocean as well as the Alfvénic plasma interaction with its ionosphere and induced field. Inhomogeneities in Europa's ionosphere at various length scales generate substantial asymmetries in the mass loading process that further complicate the structure of the moon's electromagnetic environment. In our study, the electromagnetic fields near Europa are obtained from an established hybrid model, whereas a particle tracing tool is applied to analyze the precipitation of the three most abundant energetic ion species (hydrogen, oxygen, and sulfur) onto the moon's surface at various energies from 1 keV up to 5 MeV. To isolate the contributions of the induced dipole and ionospheric mass loading to the field perturbations and the resulting precipitation patterns, we consider multiple field configurations of successively increasing complexity. For ion energies in the kiloelectron volt regime, magnetic field line draping effectively shields large portions of Europa's surface against energetic ion impacts and drastically alters the shape of the precipitation patterns, compared to uniform fields. The fine structure of these patterns strongly depends on the complexity of the applied ionosphere model. Only in the megaelectron volt regime, the precipitation patterns are qualitatively similar for uniform and draped fields. However, the precipitation of megaelectron volt ions onto Europa is still not homogeneous, since the strong magnetospheric field keeps ion gyroradii much smaller than the moon's radius.

### 1. Introduction

The orbit of Jupiter's smallest Galilean moon Europa (radius  $R_E = 1,561$  km) is located deep within the giant planet's magnetosphere at a distance of  $9.38R_J$  (radius of Jupiter:  $R_J = 71,492$  km). Geophysical models of Europa's interior suggest that the moon possesses a liquid water ocean beneath its icy crust. The energy required to keep such an ocean layer liquid is provided by tidal heating due to Europa's orbital resonance with its neighbors Io and Ganymede (Spohn & Schubert, 2003). Possessing an inclination of only  $0.47^\circ$ , Europa's orbit is located within Jupiter's (rotational) equatorial plane. However, since Jupiter's magnetic moment is tilted by  $9.6^\circ$  against the planet's rotation axis, Jupiter's intrinsic magnetic field exhibits strong oscillatory variations at the orbit of Europa. The period of these oscillations is on the order of 11.25 hr (e.g., Seufert et al., 2011). Several studies found that the secondary fields induced in the subsurface ocean by this ambient magnetic variability are strong enough to generate measurable distortions of the magnetospheric field outside of Europa (e.g., Khurana et al., 1998; Kivelson et al., 1999). Zimmer et al. (2000) demonstrated that these induced fields can best be represented by a time-varying dipole moment, centered at the moon.

Apart from the induction effect, the magnetospheric field outside of Europa is also perturbed by the interaction of the moon with Jupiter's corotating (thermal) magnetospheric plasma. Since Europa's orbital period is significantly larger than Jupiter's rotation period, the moon is continuously overtaken by the (at least partially) corotating plasma at a relative velocity of about 100 km/s (Kivelson et al., 2009). Thus, Europa represents an obstacle to the incident magnetospheric flow. Although Europa is devoid of an internally generated dynamo field (Schilling et al., 2004), the deflection of the incident plasma by the moon's induced dipole moment gives rise to additional currents and associated magnetic perturbations.

Another major contribution to these plasma currents arises from the interaction between the thermal magnetospheric flow and Europa's dilute atmosphere (e.g., Plainaki et al., 2018). The moon's gas envelope is

partially ionized, mainly through electron impacts (Saur et al., 1998). Mass loading from the resulting ionosphere leads to a deceleration and deflection of the incident magnetospheric flow as well as pileup and draping of the magnetic field (e.g., Kabin et al., 1999; Rubin et al., 2015). While the induction signal from the subsurface ocean is clearly visible in magnetic field data when Europa is located away from the center of Jupiter's plasma sheet, the plasma interaction may completely obscure the induction effect when Europa is located close to Jupiter's magnetic equator (Kivelson et al., 1999).

Since the magnetospheric plasma incident upon Europa is sub-Alfvénic, the transverse currents generated in the moon's ionosphere are closed by the currents along the characteristics of an Alfvén wing, that is, a nonlinear system of standing Alfvén waves that connects Europa to Jupiter's polar ionosphere (Neubauer, 1998). As shown by Neubauer (1999) and Volwerk et al. (2007), Europa's plasma interaction and the internal induction effect are coupled to each other: The induced field reduces the cross sections of the Alfvén wing tubes and also generates a slight displacement of the wings with respect to the moon. The maximum current which can flow along the wings is diminished as well when the induction effect is nonnegligible. In addition, Europa's Alfvén wings are modified by transient plumes of water vapor that were observed at the moon's surface (e.g., Roth et al., 2014; Sparks et al., 2016). Based on a magnetohydrodynamic simulation, Blöcker et al. (2016) demonstrated that a plume at, for example, Europa's south pole would generate a tube-like region of increased current density within the moon's southern Alfvén wing (referred to as an *Alfvén winglet*). Due to the translational invariance of the Alfvén wings along their characteristics (Neubauer, 1998), these asymmetries are still observable at large distances to Europa. Signatures of such plume-plasma interactions at Europa were recently identified in Galileo magnetometer data from the E12 and E26 flybys (Arnold et al., 2019; Jia et al., 2018).

In addition to the thermal magnetospheric plasma (which has energies on the order of  $E \approx 0.1$  keV), the plasma near Europa contains a population of high-energy ions and electrons which range in energy from  $E = 1$  keV to above  $E = 10$  MeV and are trapped in Jupiter's magnetic field (Nordheim et al., 2018; Ip et al., 1998; Paranicas et al., 2000, 2002, 2009). Since the number density of these energetic particles is by several orders of magnitude lower than that of the thermal plasma (Mauk et al., 2004), their contribution to the currents and hence the magnetic field perturbations near Europa is negligible. Therefore, the energetic population can be described as test particles that are exposed to a predefined electromagnetic field configuration. Nonetheless, the bombardment of Europa with these particles has a tremendous influence on the moon's surface and space environment. For instance, Paranicas et al. (2001) suggested that asymmetries in the flux of energetic *electrons* onto Europa's surface are the major cause of the  $\text{H}_2\text{SO}_4$  patterns seen in the moon's trailing hemisphere by Galileo. In addition, sputtering of Europa's surface by energetic *ions* was found to be the principal agent for the generation of the moon's dilute atmosphere (e.g., Plainaki et al., 2013, 2018), consisting mainly of molecular oxygen (e.g., McGrath et al., 2009). Ultimately, the fraction of sputtered surface molecules that escapes Europa's gravity also forms the extended neutral gas torus along the moon's orbit; that is, Europa's surface serves as a source of particles for the Jovian magnetosphere (Johnson et al., 2009).

To understand the spatial distribution of surface erosion at Europa, Pospieszalska and Johnson (1989) calculated the trajectories of 30-keV sulfur ions in the magnetic field near Europa and the resulting bombardment pattern of the moon's surface. They found that the intensity of energetic ion bombardment maximizes near the apex of Europa's trailing (ramside) hemisphere and decreases when moving into the leading (wake-side) hemisphere. Pospieszalska and Johnson (1989) took into account gyration of the sulfur ions around a constant magnetic field near Europa. However, their calculations did not consider the deformation of the field lines due to deflection of the incident plasma around Europa's ionosphere. The existence of Europa's induced dipole moment was not known at the time when this study was conducted.

In a similar way, Cassidy et al. (2013) used a particle tracer to study the trajectories of the three most abundant energetic ion species near Europa ( $\text{H}^+$ ,  $\text{O}^{2+}$ , and  $\text{S}^{3+}$ ; see Cooper et al., 2001 and Mauk et al., 2004) and computed surface precipitation maps for ions of different energies. These authors demonstrated that with increasing ion energy, the parallel velocity of the ions (along the magnetic field lines) becomes much larger than their drift velocity along the corotational flow direction. Therefore, Europa's north and south polar regions become more and more accessible to the incident ions. Cassidy et al. (2013) also converted their ion impact maps into profiles of the local sputtering rates and found a correlation of these rates to the observed grain size of water ice regolith at Europa's surface. However, similar to Pospieszalska and Johnson (1989),

the model of Cassidy et al. (2013) treats the magnetic field near Europa as constant; that is, the induced dipole moment and the deformation of the field lines due to plasma currents are neglected.

Paranicas et al. (2000) presented first observational hints that the magnetic pileup region upstream of Europa affects energetic ion dynamics by partially deflecting the incident ions around the moon. However, the influence of the thermal plasma interaction on energetic particle dynamics near the Galilean moons has so far been modeled only for Ganymede and Callisto. By combining a hybrid (kinetic ions and fluid electrons) model of Ganymede's thermal plasma interaction with a particle tracer for the energetic ions, Fatemi et al. (2016) and Poppe et al. (2018) showed that energetic ion precipitation onto Ganymede's surface may be a possible reason for the observed asymmetries in the moon's surface brightness. Liuzzo et al. (2019) applied a similar combination of a hybrid model (Liuzzo et al., 2015, 2016, 2017, 2018) and energetic particle tracing to study the deflection of energetic ions in the vicinity of Callisto. These authors found that Callisto's induced dipole causes energetic ion impacts to cluster in the two regions where the superposition of the induced dipole and the magnetospheric field is perpendicular to the moon's surface. Liuzzo et al. (2019) also demonstrated that the field perturbations generated by the interaction between Callisto's ionosphere/induced dipole and Jupiter's thermal magnetospheric plasma drastically alter the precipitation pattern of the energetic ions. Especially, they found that the "protection" of Callisto's surface by the ramside magnetic pileup region and the Alfvén wings almost completely shields the moon's ramside hemisphere (between 180°W and 360°W longitude) from energetic ion impacts. The perturbed electromagnetic fields also give rise to complex fine structures in the precipitation pattern that do not occur without plasma currents (see, e.g., Figure 10 of Liuzzo et al., 2019). The conclusions of Liuzzo et al. (2019) are consistent with the findings of Roussos et al. (2012), Krupp et al. (2013), Kotova et al. (2015), and Regoli et al. (2016), who constrained the contribution of the thermal/Alfvénic plasma interaction to energetic particle deflection at Saturn's moons Dione, Rhea, and Titan.

Despite their importance at Ganymede (Fatemi et al., 2016; Poppe et al., 2018) and Callisto (Liuzzo et al., 2019), there is so far no model available that considers the influence of plasma interaction currents near Europa on energetic ion dynamics. In particular, the most advanced model currently available (Cassidy et al., 2013) completely neglects the magnetic field perturbations due to flow deflection around the moon. Their model also assumes that the time-varying component of the magnetospheric field parallel to Europa's orbital plane is canceled at *all* points of the surface by the induced dipole. However, this is indeed only true when *averaging* over a full synodic rotation period of Jupiter (Saur et al., 2010; Zimmer et al., 2000), but *not* for an arbitrary distance between Europa and the center of Jupiter's magnetospheric current sheet. Thus, the results of (Cassidy et al., 2013) can (at best) be considered an estimation of the *average* precipitation pattern during one full synodic rotation of Jupiter. Only for energetic electrons, the inhomogeneities in the ambient magnetic field generated by Europa's induced dipole have been taken into account by the model of Truscott et al. (2011).

Therefore, the goal of our study is to constrain the influence of the electromagnetic field perturbations near Europa on the dynamics of energetic magnetospheric ions and on the spatial distribution of their precipitation onto the moon's surface. Especially, we will investigate how the various contributions to the field perturbations near Europa map into the precipitation pattern of energetic ions. Since Europa's exosphere is mainly generated by magnetospheric particle precipitation, constraining the "efficiency" of surface shielding by the draped electromagnetic fields is most important for understanding the moon's role as a particle source within its parent planet's magnetosphere. In particular, we aim to determine the energy range where Europa's surface is "easiest to reach" for magnetospheric ions and therefore which component of the impinging plasma population plays the predominant role in the erosion of the moon's surface.

Our modeling study is based on a combination of the electromagnetic field output from an established hybrid model (Arnold et al., 2019) and a particle tracing tool (Liuzzo et al., 2019) for the energetic magnetospheric ions. This paper is organized as follows: In section 2 we introduce the hybrid simulation code AIKEF (Arnold et al., 2019; Müller et al., 2011) and the particle tracing code GENTOO (Liuzzo et al., 2019) that are applied to study energetic ion precipitation onto Europa. We also introduce a series of model scenarios that allow to systematically constrain the influence of the various sources of field perturbations near Europa on the ion precipitation patterns. Section 3 analyzes the resulting precipitation patterns of energetic ions onto the moon's surface. The study concludes with a summary of our major findings in section 4.

Throughout this study, we apply two different coordinate systems. The electromagnetic fields from the hybrid code are given in the Cartesian EPhiO system  $(x, y, z)$ , the origin of which coincides with the center of Europa. The  $(+x)$  axis is aligned with the direction of corotation, whereas the  $(+y)$  axis points from Europa toward Jupiter. The  $(+z)$  axis completes the right-handed set and is parallel to Jupiter's rotation axis. To illustrate the precipitation of energetic magnetospheric ions onto Europa's surface, we introduce a longitude/latitude system: In Europa's equatorial plane ( $z = 0$ ), a west longitude of  $0^\circ\text{W}$  corresponds to  $(x = 0, y = +1R_E)$ , whereas longitudes of  $90^\circ\text{W}$ ,  $180^\circ\text{W}$ , and  $270^\circ\text{W}$  refer to points  $(x = +1R_E, y = 0)$ ,  $(x = 0, y = -1R_E)$ , and  $(x = -1R_E, y = 0)$ , respectively. Europa's equator is located at a latitude of  $0^\circ$ , while the moon's north  $(x = 0, y = 0, z = +1R_E)$  and south  $(x = 0, y = 0, z = -1R_E)$  poles are assigned latitudes of  $90^\circ\text{N}$  and  $90^\circ\text{S}$ , respectively.

## 2. Model Description

### 2.1. Hybrid Simulation Code AIKEF

To calculate the three-dimensional structure of Europa's electromagnetic environment, we apply the hybrid simulation code AIKEF (Müller et al., 2011), which treats the ions as individual macroparticles and the electrons as a massless, charge-neutralizing fluid. The gyroradii of the thermal magnetospheric ions at Europa are on the order of only 50 km, which is about a factor of 30 smaller than the radius of the moon. Therefore, the large-scale structure of Europa's interaction region can be captured by magnetohydrodynamic models fairly well (e.g., Kabin et al., 1999); that is, the application of a hybrid code to Europa's plasma interaction is not imperative. However, the scales of a localized plume source (e.g., Roth et al., 2014) may be comparable to ion gyroradii. Besides, the results of Blöcker et al. (2016) and Jia et al. (2018) indicate that any reasonable model of plume-plasma interactions at Europa needs to take into account the ionospheric Hall effect within the plumes (as done by AIKEF).

The AIKEF code has already been applied for extensive studies of moon-magnetosphere interactions at Europa (Arnold et al., 2019), Callisto (Liuzzo et al., 2015, 2016, 2017, 2018), and various moons visited by the Cassini spacecraft in the Saturnian system (e.g., Feyerabend et al., 2015, 2016; Krieger et al., 2009, 2011, 2014; Simon et al., 2012). Therefore, only a brief overview of the code setup for our Europa simulations is given here. For further details, the reader is referred to our preceding Europa study (Arnold et al., 2019). Any parameters not listed here (especially regarding Europa's atmosphere and ionosphere) are identical to those selected for the model runs of Arnold et al. (2019). To systematically assess the influence of inhomogeneities in Europa's electromagnetic environment on energetic ion dynamics, we will consider five field configurations of increasing complexity. We note that in the first two scenarios, the fields can be prescribed through an analytical expression and using the AIKEF code is therefore not required.

Scenario # 1 serves as a "baseline" and does not consider any plasma interaction currents at all. We set the magnetospheric field near Europa to a spatially uniform vector of  $\underline{B}_0 = (0, 0, -450)$  nT (adapted from Table 1 of Blöcker et al., 2016); that is, the field is directed southward. This orientation occurs when Europa is located near the center of Jupiter's magnetospheric current sheet. Since the horizontal component of the magnetospheric background field is 0, the magnetic moment induced in Europa's subsurface ocean disappears as well (Zimmer et al., 2000). The uniform electric field is set to  $\underline{E}_0 = -\underline{U}_0 \times \underline{B}_0$ , where  $\underline{U}_0 = (100, 0, 0)$  km/s is the upstream velocity of the thermal plasma in Europa's rest frame (e.g., Kivelson et al., 2009).

While Scenario # 2 still does not take into account any plasma interaction effects, it does consider the dipole field induced in Europa's subsurface ocean. The magnetospheric background field is set to uniform values of  $\underline{B}_0 = (0, -210, -450)$  nT (again adapted from Table 1 of Blöcker et al., 2016), corresponding to Europa being located north of the center of Jupiter's magnetospheric current sheet. According to equation (1) in Liuzzo et al. (2016), this magnetic field is associated with an induced dipole moment parallel to the  $(+y)$  axis. The electric field outside of Europa is obtained from  $\underline{E}_0 = -\underline{U}_0 \times \underline{B}$ , where  $\underline{U}_0$  again represents the undisturbed corotational flow velocity but  $\underline{B}$  denotes the *superposition* of the magnetospheric background field  $\underline{B}_0$  and the induced dipole field. Analogous to our companion Callisto study (Liuzzo et al., 2019), this setup allows to constrain the contribution of the static, induced dipole field to energetic ion dynamics near Europa. However, we also note that at Callisto, the superposition of the magnetospheric background field and the induced dipole is already sufficient to explain Galileo magnetic field observations from flybys that occurred at large distances to the Jovian current sheet, such as C3 and C9 (e.g., Kivelson et al., 1999; Liuzzo et al., 2015). For similar flybys of Europa, such a superposition was found suitable to reproduce only the observed  $B_x$  and  $B_y$ .

signatures. The perturbations seen by Galileo in  $B_z$  and  $|B|$  contain additional compression/rarefaction signatures that are generated by plasma currents and cannot be explained by taking into account the induced field alone (see, e.g., Figure 4 in Zimmer et al., 2000). Therefore, while more realistic than Scenario # 1 and the approach of Cassidy et al. (2013), the applicability of Model Setup # 2 to Europa is still somewhat limited.

Scenario # 3 includes the same background field  $B_0$ , upstream flow speed  $U_0$ , and induced dipole field as Case # 2. However, we now apply the AIKEF model to calculate the field perturbations generated by the interaction of the thermal upstream flow with Europa's induced field and its atmosphere/ionosphere. The thermal upstream ions possess a mass of 18.5 amu and a number density of  $60 \text{ cm}^{-3}$ . The temperatures of ions and electrons in the upstream flow are set to the same value of  $kT = 100 \text{ eV}$  (Kivelson et al., 2009). Europa's global atmosphere is assumed to be spherically symmetric, using the barometric profile and parameters detailed in section 2 of Arnold et al. (2019). In addition, this scenario includes a localized plume of water vapor emanating from Europa's south pole  $(x, y, z) = (0, 0, -1R_E)$ , with the plume axis being aligned with the  $z$  axis and plume parameters from section 2 of Arnold et al. (2019).

As can be seen in Figures 1a and 1b, the plasma interaction in Scenario # 3 generates magnetic field pileup upstream of Europa as well as a set of Alfvén wings, with the south polar plume causing only a very subtle north-south asymmetry in the  $B_x$  perturbations and the pileup region. However, mass loading by freshly produced plume ions generates an extended region of reduced (thermal) plasma velocity south of Europa, the size of which even exceeds that of the moon itself (see Figure 1c). As displayed in Figure 1d, this region of nearly stagnant flow also maps into the electric field  $E$  and reduces the field magnitude above Europa's south pole to  $\approx 10\%$  of the background value. Since Europa's ionosphere is mainly populated by nearly stagnant plasma, the electric field within the moon's gas envelope is reduced in a similar way. However, the scale height of Europa's global atmosphere in the model is on the order of only 3% of the moon's radius, whereas the scale height of the south polar plume is about a factor of 4 larger (Arnold et al., 2019). Therefore, the extension of the electric field void encapsulating the moon is small compared to the extended south polar depletion of  $|E|$ . The small extension of the "global" electric field void around the moon is a major difference to the field configuration in our preceding Callisto study (Liuzzo et al., 2019) and will be shown to cause substantial differences in the precipitation patterns of energetic ions at both moons.

While Scenario # 3 is suitable to illustrate how mass loading from Europa's ionosphere affects the electromagnetic fields and energetic ion precipitation, the setup is still somewhat idealized: The  $B_x$  component of the magnetospheric background field is set to 0, Europa's global atmosphere is assumed to be symmetric between its leading and trailing hemispheres, and the plume location was not chosen to match a specific set of observations. In the final step of our study, we therefore consider energetic ion dynamics at Europa for a fully realistic thermal plasma interaction. More specifically, our Model Scenario # 4 is based on the electromagnetic fields calculated by Arnold et al. (2019) for the E26 flyby. Their model takes into account the background field observed by the Galileo magnetometer,  $B_0 = (-22, 205, -379) \text{ nT}$ , as well as the associated induced magnetic moment. In addition to the leading-trailing asymmetry of Europa's global atmosphere, their model also considers a local plume source in Europa's southern trailing hemisphere, the axis of which is inclined against the local zenith direction. As shown by Arnold et al. (2019), inclusion of this plume source was required to achieve quantitative agreement between modeled and observed time series of the magnetic field along Galileo's trajectory. The setup of our Scenario # 4 is identical to Run 1 of Arnold et al. (2019).

While the asymmetries of Europa's global atmosphere were found to have only minor quantitative effect on the moon's thermal plasma environment (Rubin et al., 2015 and Figure 2c of Arnold et al., 2019), the influence of a compact and localized plume source on the fields appears to be quite drastic and discernible way outside of the plume (e.g., Figure 1 of this study and Blöcker et al., 2016; Jia et al., 2018). Therefore, we shall investigate in more detail how such a plume source affects the energetic ion precipitation pattern. To isolate the influence of the plume on energetic ion precipitation, we consider a "clone" of Scenario # 4 with all upstream and global atmospheric parameters unaltered, but the plume source removed. Thus, the electromagnetic field perturbations in this Scenario # 5 are identical to those in Run 5 of Arnold et al. (2019). We note that this model setup no longer achieved quantitative agreement with the fine structures in the observed magnetic field, but it was merely introduced in our preceding study to substantiate the hypothesis of a plume detection during E26.

Europa's electromagnetic environment in Model Scenarios # 4 and # 5 is qualitatively similar to Figure 1, and a detailed discussion can be found in our preceding publication.

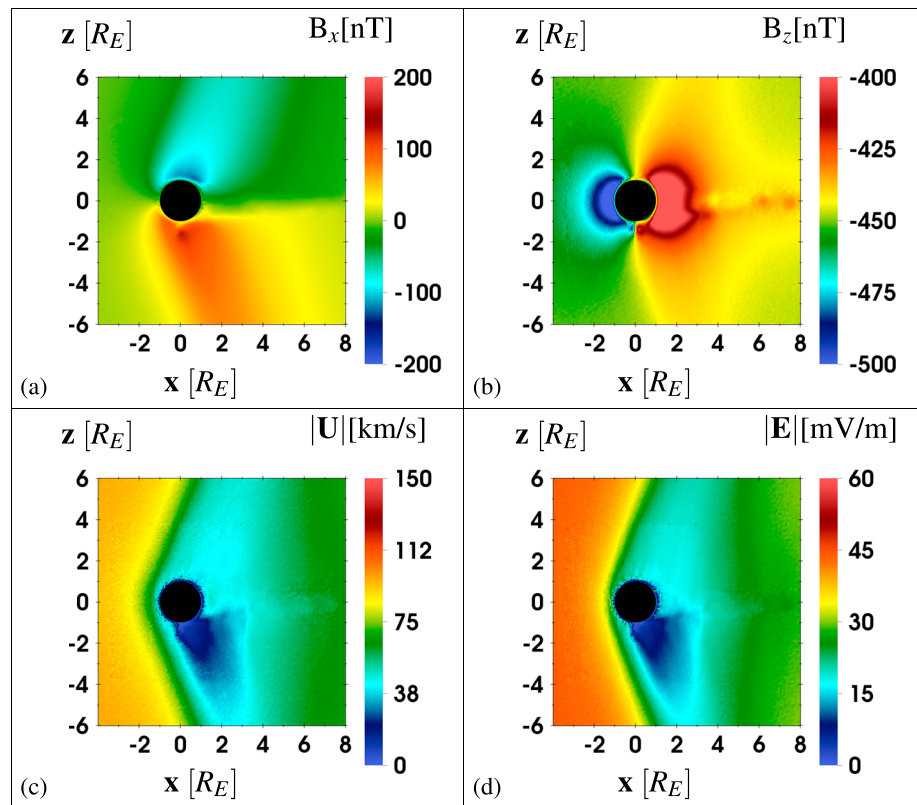


**Figure 1.** Europa’s electromagnetic and thermal plasma environment for the interaction parameters of Scenario # 3. For the  $(x, z)$  plane of the EPhiO system, the figure displays (a) the magnetic field component  $B_x$  along the corotation direction, (b) the magnetic field component  $B_z$  in the (geographic) north-south direction, (c) the bulk velocity  $|\underline{U}|$  of the plasma, and (d) the magnitude of the electric field  $|\underline{E}|$ .

In summary, our selection of model setups allows to isolate the influence of all key components of Europa’s thermal plasma interaction on energetic ion dynamics. A comparison between Scenarios # 1 and # 2 facilitates the identification of features in the precipitation patterns that are caused by the induced dipole moment alone. Scenarios # 3 and # 4 are suitable to demonstrate how mass loading from Europa’s ionosphere (including a local plume source) affects the baseline picture obtained from Cases # 1 and # 2. Finally, Scenario # 5 allows to constrain the scales upon which a local atmospheric inhomogeneity alters the ion precipitation pattern in a fully realistic interaction geometry, as observed by Galileo. Key parameters of all five model setups are summarized in Table 1.

**Table 1**  
Key Parameters of Europa’s Electromagnetic Environment in Scenarios # 1 to # 5

Model setup	Scenario				
	# 1	# 2	# 3	# 4	# 5
Thermal plasma interaction?	no	no	yes	yes	yes
Induced dipole?	no	yes	yes	yes	yes
Global atmosphere?	no	no	symmetric	asymmetric	asymmetric
Plume?	no	no	south polar	E26, southern trailing hemisphere	no
Background magnetic field	(0, 0, -450) nT	(0, -210, -450) nT	(0, -210, -450) nT	E26, (-22, 205, -379) nT	E26, (-22, 205, -379) nT
Upstream plasma velocity	(100, 0, 0) km/s	(100, 0, 0) km/s	(100, 0, 0) km/s	(100, 0, 0) km/s	(100, 0, 0) km/s
Upstream plasma density	n/a	n/a	60 cm <sup>-3</sup>	30 cm <sup>-3</sup>	30 cm <sup>-3</sup>

*Note.* The abbreviation “E26” implies that the respective parameter has been adapted from the E26 model of Arnold et al. (2019). n/a = not applicable.

## 2.2. Particle Tracing Model GENTOO

To analyze the dynamics of energetic magnetospheric ions near Europa, we use the GENTOO particle tracing model originally developed by Liuzzo et al. (2019) for Callisto. GENTOO applies a Runge-Kutta scheme of fourth order to calculate the trajectories of energetic ions in the stationary electromagnetic fields from the AIKEF hybrid model. In principle, the energetic component of the upstream plasma could be included in the AIKEF model in a self-consistent way. However, since the time step  $\Delta t$  of AIKEF is limited by the Courant-Friedrichs-Lewy condition (Müller et al., 2011), inclusion of a particle population in the kiloelectron volt to megaelectron volt regime would require a reduction of the time step beyond feasibility. Hence, this approach does not take into account the weak contribution of the energetic ions to the electromagnetic field perturbations near Europa. In the following, we briefly outline several key elements of the GENTOO model. A far more comprehensive description can be found in section 2.2 of our aforementioned Callisto study (Liuzzo et al., 2019). A predecessor of GENTOO was applied by Regoli et al. (2016) to study energetic ion precipitation onto Titan's exobase, where further details of the model are discussed.

In this study, we analyze the dynamics and surface precipitation of energetic  $H^+$ ,  $O^{2+}$ , and  $S^{3+}$  ions, which have been observed by Galileo's *Energetic Particles Detector* (EPD) during multiple close flybys of Europa (e.g., Cooper et al., 2001; Paranicas et al., 2009). The charge states of the two heavy ion species have been chosen in agreement with Voyager and Ulysses observations in Jupiter's middle magnetosphere (e.g., Collier & Hamilton, 1995; Keppler & Krupp, 1996) and are also consistent with the model of Cassidy et al. (2013), thereby facilitating a direct comparison to the results of that study. However, we note that there is an ongoing debate on the charge states of heavy ions in Jupiter's magnetosphere. Clark et al. (2016) showed that charge states are not uniform but have a distribution. N nnon and Andr  (2019) demonstrated that energetic ion charge states likely evolve with energy and distance from Jupiter. Selesnick and Cohen (2009) suggest that at the highest energies, heavy ions may be fully ionized.

To avoid calculating the trajectories of ions that do not even enter the vicinity of Europa, GENTOO traces particle motion backward in time: Ions of a given energy are initialized at the surface of the moon and Newton's equations of motion for each ion are solved using a negative time step  $\Delta t < 0$ . In analogy to Liuzzo et al. (2019), we consider ion energies in the range of  $1 \text{ keV} \leq E \leq 5 \text{ MeV}$ , which covers the entire regime where Galileo detected nonnegligible energetic ion fluxes near Europa (e.g., Paranicas et al., 2000, 2009). In this energy range, the relativistic mass growth of the ions does not need to be considered.

Each GENTOO run computes the trajectories of about 65 million ions. Similar to Regoli et al. (2016) and Liuzzo et al. (2019), we define a spherical starting grid on the surface of Europa with a resolution of  $2^\circ$  in latitude and  $4^\circ$  in longitude. At each of these  $90^2 = 8,100$  grid points, individual ions of a given velocity  $v = \sqrt{2E/m}$  are launched at discrete angles with respect to the local surface normal. In velocity space, we again use a resolution of  $2^\circ$ , measured against the local surface normal and  $4^\circ$  along the azimuthal direction, yielding 8,100 ions launched from each point on Europa's surface. To isolate the contributions of different ion species (i.e., different mass-to-charge ratios) and energies to surface precipitation, each run considers only a *single* species and energy.

The AIKEF model (like any local plasma interaction model) can be applied to calculate the electromagnetic field perturbations only within a box of size  $\approx \pm 20R_E$  in each direction, centered at Europa. At this distance, the electromagnetic field perturbations generated by Europa have either faded away or are highly localized within the two Alfv nic fluxtubes. However, during its motion an energetic ion may leave Europa's local environment and—in an extreme case—follow the magnetic field lines all the way to Jupiter's polar ionosphere, bounce back and then (half a bounce period  $\tau_b/2$  later) reenter Europa's interaction region farther downstream. Paranicas et al., 2000 (2000, 2009) estimated  $\tau_b/2$  for various energetic ion species and found it to be significantly larger than the contact time of the magnetic flux tubes when passing Europa in azimuthal direction: for instance, a 1-MeV oxygen ion near Europa's orbit has a half-bounce period of  $\tau_b/2 = 343 \text{ s}$ , whereas the magnetic field line around which it gyrates requires only 27.82 s to travel a distance of  $2R_E$ . The gyroradius of the oxygen ion is on the order of only  $0.5R_E$  (see Table 2 of Paranicas et al., 2009). Thus, once such a bouncing ion has left Europa's local environment to travel toward Jupiter, it will return to Europa's orbit about  $20R_E$  downstream; that is, it is no longer able to interact with the moon. Therefore, our particle tracing model does not require inclusion of a full model of Jupiter's magnetospheric field. Instead, we shall adapt the approach of Regoli et al. (2016), Kabanovic et al. (2018), and Liuzzo et al. (2019) who treated the

electromagnetic fields outside of the hybrid simulation domain as spatially constant (using the upstream values from AIKEF).

Since the motion of an ion cannot be tracked indefinitely, several exit conditions (adopted from Regoli et al., 2016 and Liuzzo et al., 2019) have been implemented to determine whether a certain backtraced ion can contribute to surface precipitation. (i) If, at any point in time, the trajectory of the ion intersects the surface of Europa ( $\sqrt{x^2 + y^2 + z^2} = R_E$ ), it is labeled “forbidden.” When tracing the motion of a forbidden ion *forward* in time (i.e.,  $\Delta t > 0$ ), it would have to travel through the solid body of Europa in order to arrive at its “launch point” on the starting grid. Thus, a forbidden ion cannot make a contribution to surface precipitation. (ii) In principle, if the trajectory of a (backtraced) ion never intersects the surface of Europa, GENTOO would trace its motion for an arbitrarily long time. Ultimately, this time would even exceed the half-period of Jupiter’s current sheet sweeping through Europa’s orbital plane (about 5 hr); that is, the notion of constant magnetospheric upstream conditions near the moon (which is inherent to the AIKEF model) would no longer be valid. Therefore, the backtracing of an energetic ion is aborted and the particle is labeled “escaped” or “allowed,” if *both* of the following conditions are met: (ii.a) At some point in time, the backtraced ion leaves the AIKEF simulation box and begins to travel through the uniform electromagnetic fields outside. (ii.b) After the backtraced ion has exited the AIKEF domain for the first time, it needs to complete two full gyrations without hitting Europa. For Model Scenarios #1 and #2, we apply this exit condition to a hypothetical box of size  $-20R_E \leq x, y, z \leq +20R_E$ , whereas for the remaining three scenarios this condition is applied at the faces of the actual AIKEF domain with size  $\pm 20R_E$  in each direction. If the equations of motion were integrated forward in time ( $\Delta t > 0$ ), an escaped ion would be able to reach its launch point on the starting grid; that is, it would contribute to surface precipitation at that location. In analogy to Cassidy et al. (2013), our model assumes the energy loss of the energetic ions through collisions with Europa’s dilute atmosphere to be negligible.

To quantify spatial inhomogeneities in the surface precipitation pattern, Regoli et al. (2016) and Liuzzo et al. (2019) have introduced an *accessibility parameter*  $\lambda(E, x, y, z)$  for each ion species. At each point  $(x, y, z)$  of the starting grid, this parameter describes the fraction of backtraced ions (at a given initial energy  $E$ ) that possess *allowed* trajectories and can therefore contribute to surface precipitation. Thus, a value of  $\lambda = 100\%$  implies that all ions launched at a certain grid point can escape, whereas  $\lambda = 0\%$  means that none of the backtraced ions can escape and that point is completely shielded. Since the total number of newly initialized ions is the same at each point of the starting grid, a surface map of  $\lambda$  also illustrates how the absolute number of backtraced ions with allowed trajectories changes as a function of latitude and longitude.

### 3. Model Results: Accessibility of Europa’s Surface to Energetic Ions

#### 3.1. Scenario # 1: Ion Precipitation for Uniform Fields

For the case of uniform electromagnetic fields (Scenario # 1), Figure 2 displays maps of the accessibility parameter  $\lambda$  for the three energetic ion species observed near Europa. For the background field  $\underline{B}_0$  and ion energies considered here, the gyroradii are in the range of  $r_g = (0.007 - 0.46)R_E$  (hydrogen),  $r_g = (0.01 - 0.92)R_E$  (oxygen), and  $r_g = (0.01 - 0.87)R_E$  (sulfur), respectively. Thus, at the lowest energies considered, ion dynamics can almost completely be explained in terms of translation of the guiding centers, and even in the megaelectron volt regime gyration may impose only weak asymmetries on the accessibility patterns. As can be seen from Figure 2, the accessibility maps at all energies are nearly symmetric between Europa’s Jupiter-facing and Jupiter-averted hemispheres. At none of the energies considered, a backtraced ion may evade impacting Europa (and hence, become allowed) by gyrating around the moon. The weak influence of gyration on energetic ion dynamics is the major difference to Callisto where the gyroradii of oxygen and sulfur ions in the weak magnetospheric field may become more than an order of magnitude larger than the radius of the moon (see Table 2 of Liuzzo et al., 2019). In contrast to Europa, gyration of energetic ions at Callisto generates pronounced hemispherical asymmetries in the accessibility patterns even at low energies (see, e.g., Figure 4 of Liuzzo et al., 2019).

At the lowest energy considered ( $E = 1$  keV), the accessibility profiles of all three species display a pronounced asymmetry between Europa’s trailing (ramside) and leading (wakeside) hemispheres (see Figures 2a, 2f, and 2k). Since in the *backtracing* approach the  $\underline{E} \times \underline{B}$  drift is oriented in *negative*  $x$  direction (toward upstream), ions initialized at Europa’s wakeside immediately reencounter the surface of the moon and their trajectories become forbidden. For 1-keV particles the “bubble” of reduced accessibility at Europa’s

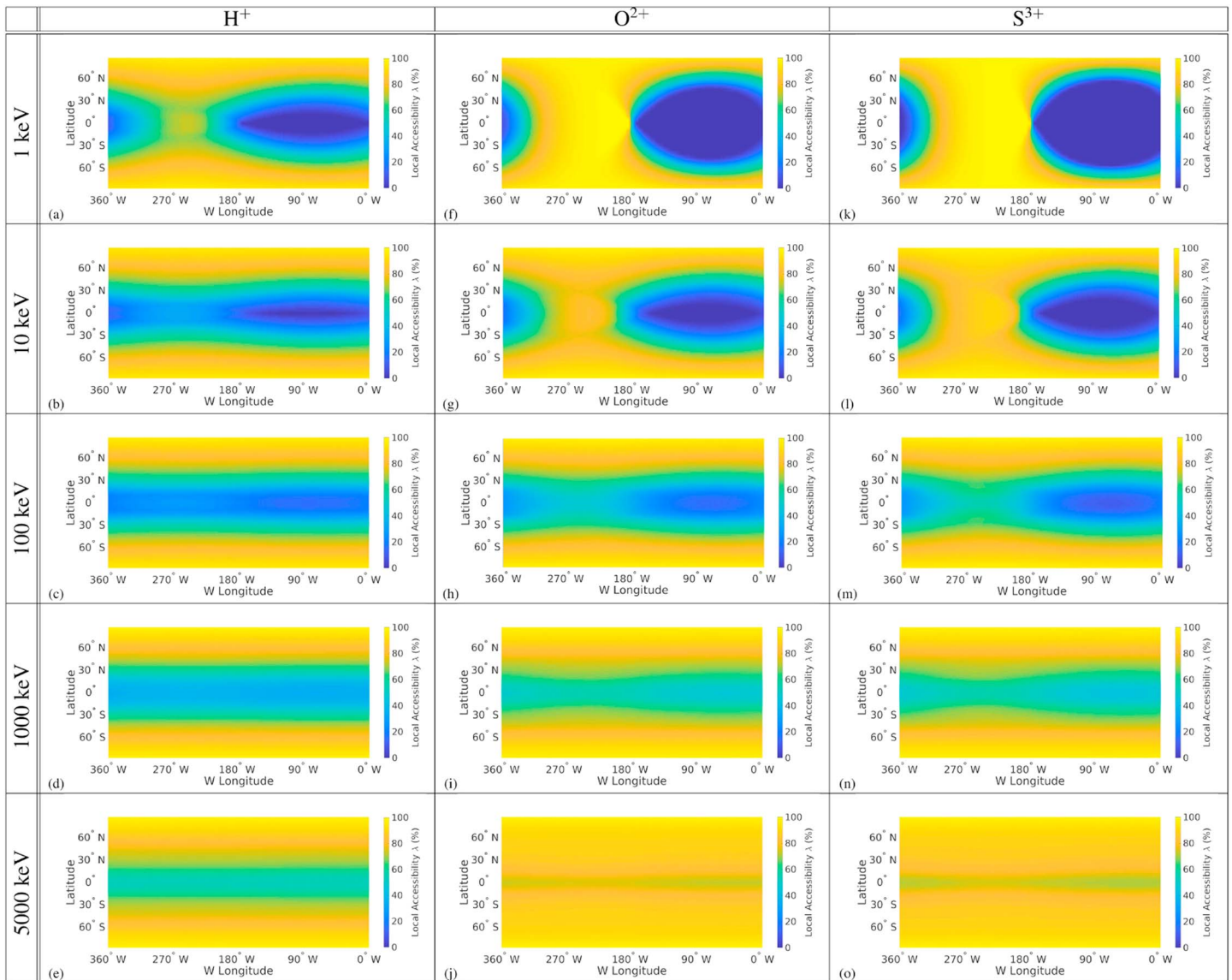


**Figure 2.** (a–o) Energetic ion accessibility of Europa’s surface for the uniform electromagnetic fields of Scenario # 1. For five discrete initial ion energies from 1 keV to 5 MeV and the three energetic ion species observed near Europa’s orbit, the panels display maps of the accessibility parameter  $\lambda$ . In each panel, longitude is displayed on the horizontal axis, and the latitude is given on the vertical axis.

wakeside grows in size with increasing ion mass. At a given energy the (parallel) velocity of the newly initialized ions *decreases* with increasing mass  $m$ , thereby facilitating the transport of the ions toward upstream by the “inverse”  $\underline{E} \times \underline{B}$  drift and their impact onto Europa’s leading hemisphere. At Europa’s ramside the drift immediately transports newly initialized ions away from the moon, causing the accessibility to peak around the 270°W meridian below energies of 100 keV (see the first and second rows of Figures 2).

Yet, near Europa’s trailing apex (270°W longitude, 0° latitude, or  $(x, y, z) = (-1R_E, 0, 0)$ ) the accessibility of 1-keV ions reaches a value of  $\lambda \approx 100\%$  only for oxygen and sulfur, whereas it remains at  $\lambda \approx 80\%$  for the light hydrogen ions. This weak disparity is indeed caused by the gyration of the backtraced ions around the uniform magnetic field. With increasing ion mass  $m$ , the (parallel) velocity of the ions at a given energy decreases with  $1/\sqrt{m}$ , whereas their gyroperiod increases with  $m$ . Thus, the distance traveled by an ion along the magnetic field during one full gyroperiod increases  $\propto \sqrt{m}$ . In other words, due to the curvature of Europa’s surface, a newly initialized proton “returns” from its first gyration closer to (or even below) the

surface than an ion of the two heavier species, thereby facilitating proton impacts that lead to forbidden trajectories around the moon's trailing apex.

With increasing ion energy, the wakeside region of reduced accessibility "collapses" into a narrow ribbon, centered around Europa's equator (bottom three rows of Figure 2). Simultaneously, accessibility around the apex of Europa's ramside hemisphere decreases as well, and at energies of 1,000 keV and 5,000 keV, the value of  $\lambda$  is slightly decreased only within a narrow belt along the moon's geographic equator. Only within this belt, the uniform magnetospheric field is (nearly) tangential to Europa's surface, thereby facilitating the impact of gyrating ions onto the moon immediately after initialization. With growing distance  $|z|$  to the equator, the magnetospheric field  $\underline{B}_0$  becomes increasingly radial to the surface, thereby allowing the escape of backtraced ions along the field lines.

In a forward-tracing approach, the dynamics of these megaelectron volt ions are mainly governed by their parallel motion and no longer by the  $\underline{E} \times \underline{B}$  drift (see also Cassidy et al., 2013). In other words, since heavy ions have relatively long bounce periods (compared to the transition time of the flow through Europa's interaction region), they tend to precipitate onto the moon from the north and the south (Paranicas et al., 2009). Hence, ions that "attempt" to impinge at low northern and southern latitudes first need to travel a distance of about  $|\Delta z| = 1 R_E$  along magnetic field lines close to Europa's surface without hitting the moon through gyration. In consequence, the incident ion population becomes increasingly depleted before reaching equatorial latitudes. Even at particle energies of 5,000 keV, the accessibility of Europa's equatorial region is still slightly reduced (see Figures 2e, 2j, and 2o), with the depletion being weakest for the species with the largest gyroradius (oxygen). At high energies, ion gyration becomes increasingly important, that is, the size of the Europa obstacle "shrinks," compared to the scales of ion motion and the surface becomes more and more accessible. Only at ion energies above 5,000 keV would Europa's surface become homogeneously accessible to the incident ion population. However, at these energies Galileo no longer observed significant energetic particle fluxes near the moon (e.g., Paranicas et al., 2009).

The setup of Scenario # 1 (uniform electromagnetic fields, no induced dipole nor plasma interaction effects) is qualitatively similar to the configuration studied by Cassidy et al. (2013). In agreement with our findings, these authors identified a pronounced ram-wake asymmetry in the precipitation pattern at energies of 1–10 keV. In addition, their results confirm that around  $E = 100$  keV Europa's polar caps become fully accessible to the incident ions and only the moon's equatorial region is still partially protected (see Figure 8 in that work).

We also note that the precise charge states of the heavy ions are not a critical parameter for our study. For instance, when "switching" from multiply charged to singly charged oxygen and sulfur ions, the gyroradii (at a given energy) merely increase by a factor of 2 (oxygen) or 3 (sulfur). Thus, the size of the Europa obstacle slightly shrinks, compared to the length scales of ion dynamics. Hence, the sequence of accessibility maps in Figure 2 would be shifted to slightly lower energies, with the shift still being smaller than the "gaps" between the discrete energies considered here. However, the exact charge states of the ions will play an important role in future studies that aim to quantitatively constrain the evolution of particle fluxes onto Europa's surface during a full oscillation of Jupiter's magnetospheric current sheet.

### 3.2. Scenario # 2: Superposition of Magnetospheric Field and Induced Dipole

The magnetospheric field in Scenario # 2 possesses a component away from Jupiter, thereby also introducing an induced magnetic moment along the (+y) axis (e.g., Zimmer et al., 2000). The accessibility maps for this scenario are displayed in Figure 3. To isolate the influence of the induced dipole field, Figure 4 shows the maps for a (hypothetical) configuration that considers only the tilted background field, but no induced dipole moment. Without the induced field, the accessibility patterns (qualitatively) contain the same features as in Scenario # 1. However, since the magnetic field is no longer aligned with the north-south axis ( $-z$ ), these features are rotated across Europa's surface, thereby generating the impression of "wavy" regions with low accessibility in the projections from Figure 4 (most clearly discernible at the highest energies).

A comparison between Figures 3 and 4 illustrates that the induced dipole mainly has a quantitative influence on the accessibility patterns. Inclusion of the induced field mainly moves regions of low accessibility closer to Europa's equator and also largely eliminates the wavy structure. The boundaries to adjacent regions of higher  $\lambda$  also become broader and somewhat blurred (see first three rows in Figures 3 and 4). As discussed

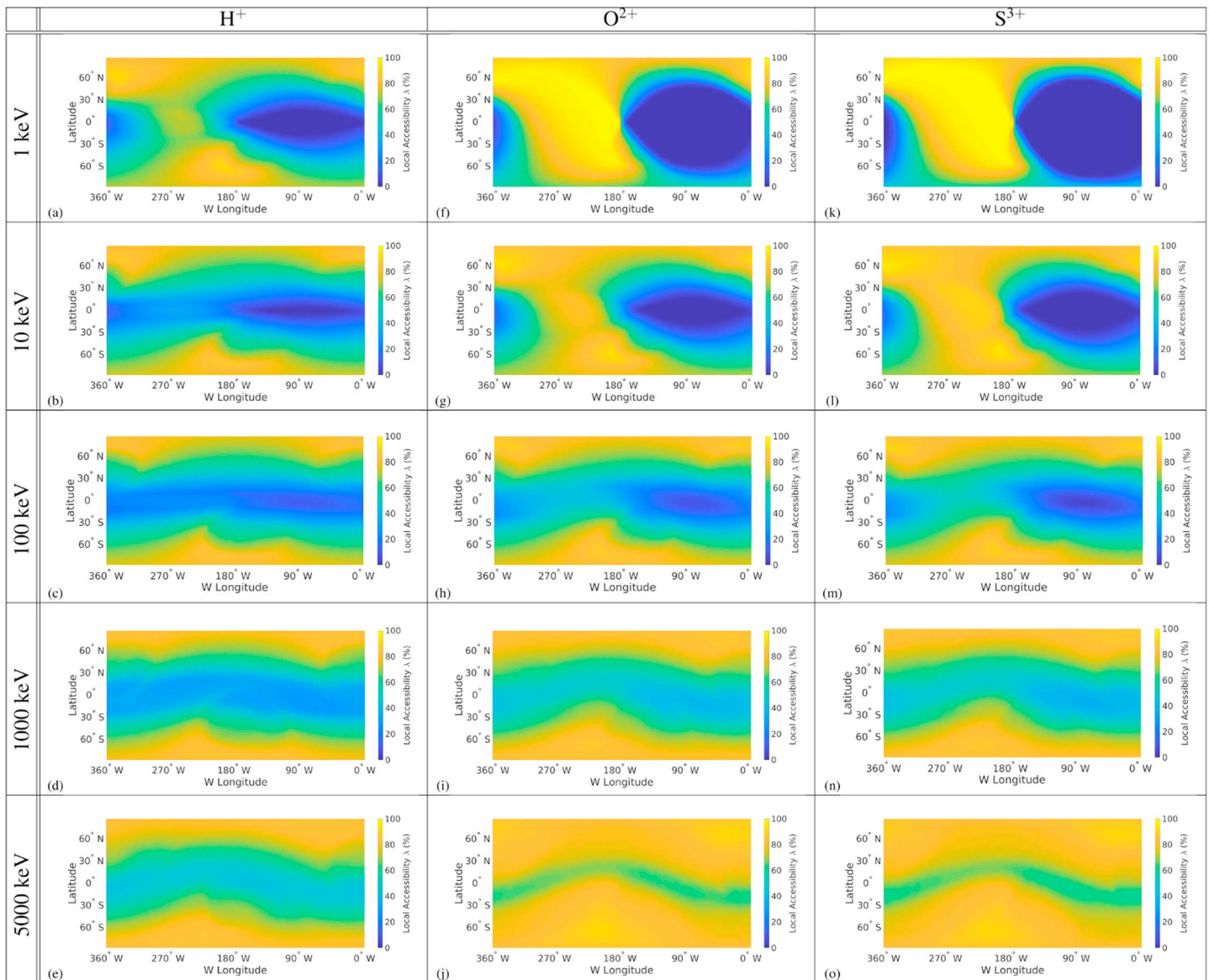


**Figure 3.** (a–o) Accessibility of Europa’s surface to energetic ions when exposed to the superposition of a (slightly inclined) magnetospheric background field  $B_0$  and the field from the induced dipole moment, pointing in (+y) direction (Scenario # 2). Panels in the same row display the accessibility  $\lambda$  for different ion species at a given energy, whereas the evolution of the accessibility patterns for each species with increasing energy is shown in the columns. Please note that the strength of the magnetospheric background field is higher than in Scenario # 1; that is, a quantitative comparison between Figure 2 and the results shown here would not be meaningful.

by, for example, Zimmer et al. (2000) and Liuzzo et al. (2019), the superposition of the induced dipole and the horizontal component  $(B_{0,x}, B_{0,y}, 0)$  of the magnetospheric field encapsulates the moon like a “cocoon”; that is, the magnetic field lines look similar to the stream lines of a hydrodynamic flow around a spherical obstacle. Thus, except for the vicinity of the two “magnetic poles” where the induced dipole field is perpendicular to Europa’s surface, the total field would possess a strong component tangential to the surface. However, when including the north-south component  $B_{0,z}$ , the resulting field is tangential to the surface only close to the moon’s geographic equator. This configuration facilitates impact of backtraced ions injected at equatorial latitudes: While translating along the field lines, their gyration drives the ions onto the surface almost immediately. Similar to Scenario # 1, the  $\underline{E} \times \underline{B}$  drift drags ions launched at the wakeside back to Europa, which explains the broad drop in accessibility between longitudes of 0°W and 180°W that can still be seen in the first three rows of Figure 3.

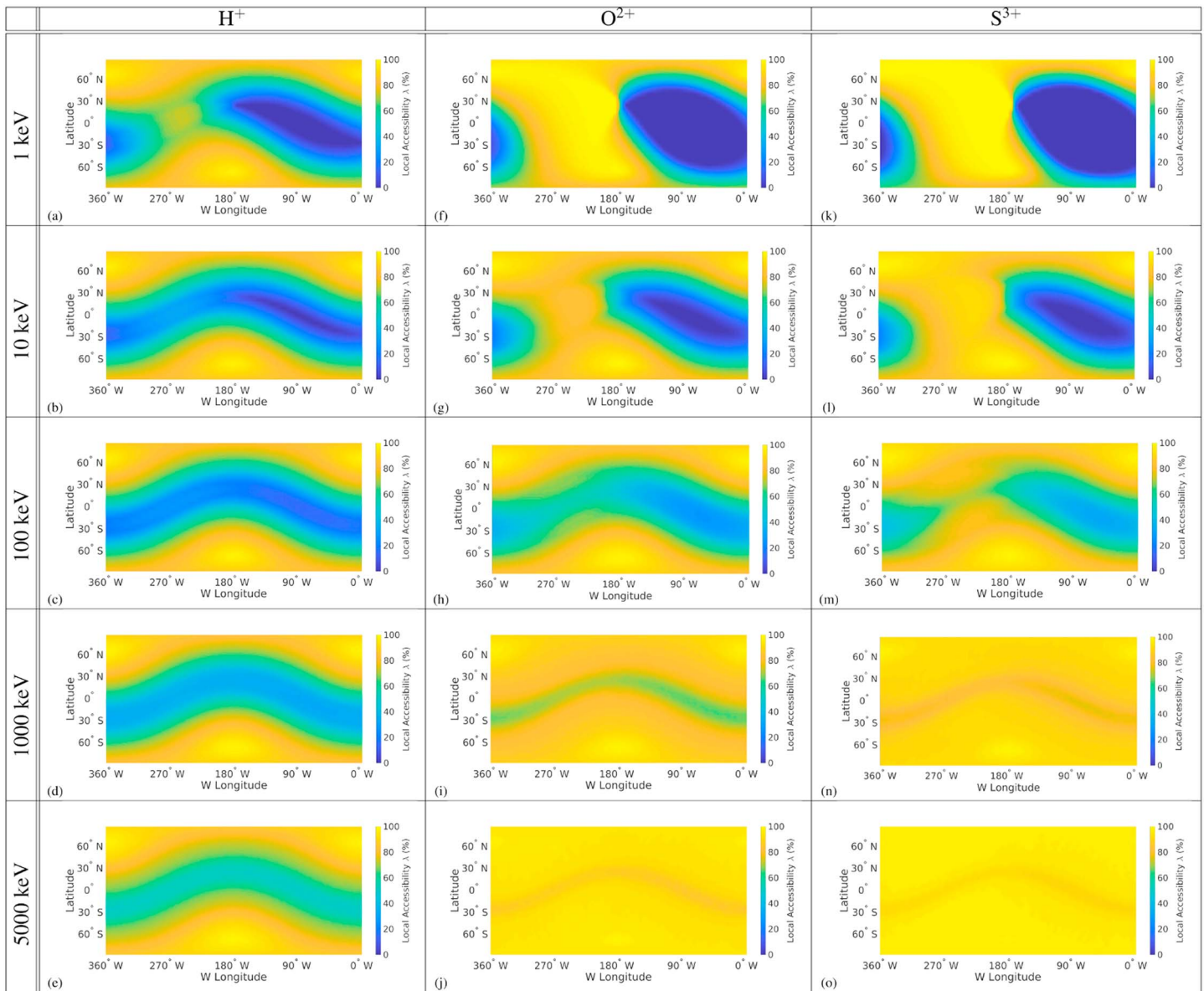


**Figure 4.** (a–o) Accessibility maps for the same magnetospheric background field orientation as in Scenario # 2, but *without* the induced dipole moment. Although this setup is somewhat artificial, it facilitates the analysis of the accessibility maps when both contributions to the magnetic field are taken into account (see Figure 3).

Most remarkably, even in the megaelectron volt regime the induced dipole field still provides some level of protection of Europa’s equatorial region against energetic ion precipitation. In particular, when only the homogeneous background field is taken into account, the accessibility of Europa’s surface to megaelectron volt oxygen and sulfur ions reaches  $\lambda \geq 90\%$  nearly everywhere (see Figures 4i, 4j, 4n, and 4o), while only about 50–60% of the backtraced ions can escape from equatorial latitudes when the induced dipole is included as well (same panels in Figure 3). Even near Europa’s geographic poles, inclusion of the induced dipole still reduces  $\lambda$  by about 15%. These disparities stem from the locally changed gyroradii when both contributions to the magnetic field are considered.

It is important to note that this partial protection of Europa’s equatorial region would not average out when considering a full synodic rotation of Jupiter. The longitudinal homogeneity of the “belt” of reduced  $\lambda$  in the two bottom rows of Figure 3 demonstrates that this effect mainly depends on the location of the induced dipole moment in the  $(x, y)$  plane of the EPhiO system. Since at Europa the  $B_{0,x}$  component is weak compared to  $B_{0,y}$  (Kivelson et al., 1999), the induced magnetic moment oscillates in magnitude during a full

synodic rotation, but it always remains (nearly) parallel/antiparallel to a straight line through  $(0, -R_E, 0)$  and  $(0, +R_E, 0)$ . Only when the center of Jupiter's magnetospheric current sheet sweeps over Europa, the induced magnetic moment briefly vanishes (Zimmer et al., 2000), thereby temporarily enhancing the exposure of the moon's equatorial region to energetic ion precipitation. However, we emphasize that this picture still does not consider any contribution of plasma interaction currents to the fields. The strength of Europa's thermal plasma interaction indeed maximizes when the moon is located near the center of the Jovian plasma sheet (e.g., Kivelson et al., 2004).

Overall, inclusion of the induced field seems to have a much weaker effect on the precipitation maps than at Callisto: As shown by Liuzzo et al. (2019), Callisto's induced magnetic moment generates quasi-circular "patches" of high accessibility around the two points where the induced moment is perpendicular to the moon's surface and nearly cancels the magnetospheric background field (see Figure 4 in that study). At Callisto, this clustering of highly accessible regions is still clearly discernible at energies in the megaelectron volt regime. A major difference between the magnetospheric environments at Callisto and Europa is the orientation of the ambient magnetospheric field. When Callisto is located outside of Jupiter's plasma sheet, the field is strongly stretched toward/away from the planet's rotation axis; that is, the  $B_{0,y}$  component is the dominant one and can become 2–3 times stronger than  $B_{0,z}$  (Kivelson et al., 1999; Liuzzo et al., 2016, 2017). However, even at large distances to the plasma sheet, the field at Europa still points mainly in north-south direction; that is,  $B_{0,z}$  dominates. The corotation-aligned magnetospheric field component  $B_{0,x}$  is negligible at both moons. The strength of the induced magnetic moment  $|\underline{M}_{\text{ind}}|$  is proportional to  $\sqrt{B_{0,x}^2 + B_{0,y}^2}$ , and it cancels only the *horizontal* component of the background field  $(B_{0,x}, B_{0,y}, 0)$  near the two points where a straight line along  $\underline{M}_{\text{ind}}$  pierces the moon's surface (Liuzzo et al., 2019). However, the  $B_{0,z}$  component of the magnetospheric background field is completely unaffected by the induced moment near these two magnetic poles and the modification of  $B_{0,z}$  everywhere else is also rather weak. Thus, in contrast to Callisto, the strongest component of the magnetospheric background field near Europa remains nearly unaffected by inclusion of the induced dipole, which explains the strong similarities of the maps in Figures 3 and 4.

Due to their similar mass-to-charge ratios, the precipitation maps of oxygen and sulfur ions display only minor quantitative differences. In a *forward-tracing* approach and at the lowest energies considered, this can also be understood as follows: A proton's corotation energy is typically on the order of 0.1 keV, while the corotation energies of oxygen and sulfur ions are 16 and 32 times larger, respectively. When traveling through the perturbed electromagnetic fields near Europa, the changes in energy of the two heavy ion species typically remain way below their corotation energy, which is why the accessibility maps look similar.

### 3.3. Scenario # 3: Influence of Europa's Thermal Plasma Interaction

The accessibility maps calculated with GENTOO for Scenario # 3 are shown in Figure 5. We emphasize again that inclusion of the plasma interaction currents is the "only" change compared to Scenario # 2; that is, the background field  $\underline{B}_0$  and the induced dipole moment are the same in both runs. The differences between the accessibility maps in Figures 3 and 5 are drastic: With the plasma currents included, the accessibility no longer comes close to  $\lambda \approx 100\%$  anywhere on Europa's surface, no matter which ion species or energy is considered. Even at an initial energy of 5 MeV, Europa's surface is still partially protected from energetic ion precipitation. However, in the megaelectron volt regime the accessibility patterns of the two heavy species are at least qualitatively similar to those seen in Figure 3, displaying a wavy band of minimum accessibility at equatorial latitudes.

Below energies of 1 MeV, large segments of Europa's surface become completely inaccessible to energetic ions. In agreement with the findings of Paranicas et al. (2000), the ramside magnetic pileup region partially protects Europa's upstream hemisphere from energetic ion precipitation. This effect is best visible at an initial energy of 1 keV, see first row in Figure 5. The region of elevated accessibility between longitudes of  $180^\circ\text{W}$  and  $270^\circ\text{W}$  that was formed without the plasma interaction (see first two rows of Figure 3) can still be identified in the maps. However, compared to Scenario # 2, this structure is displaced slightly toward the north by the wrapping of the magnetic field around Europa, and the values of  $\lambda$  have dropped by a factor of 2–3 (see the first two rows of Figure 5). The accessibility maps in Figure 5 do not display any discernible symmetry, mainly because the magnetospheric background field is inclined against the induced dipole moment.

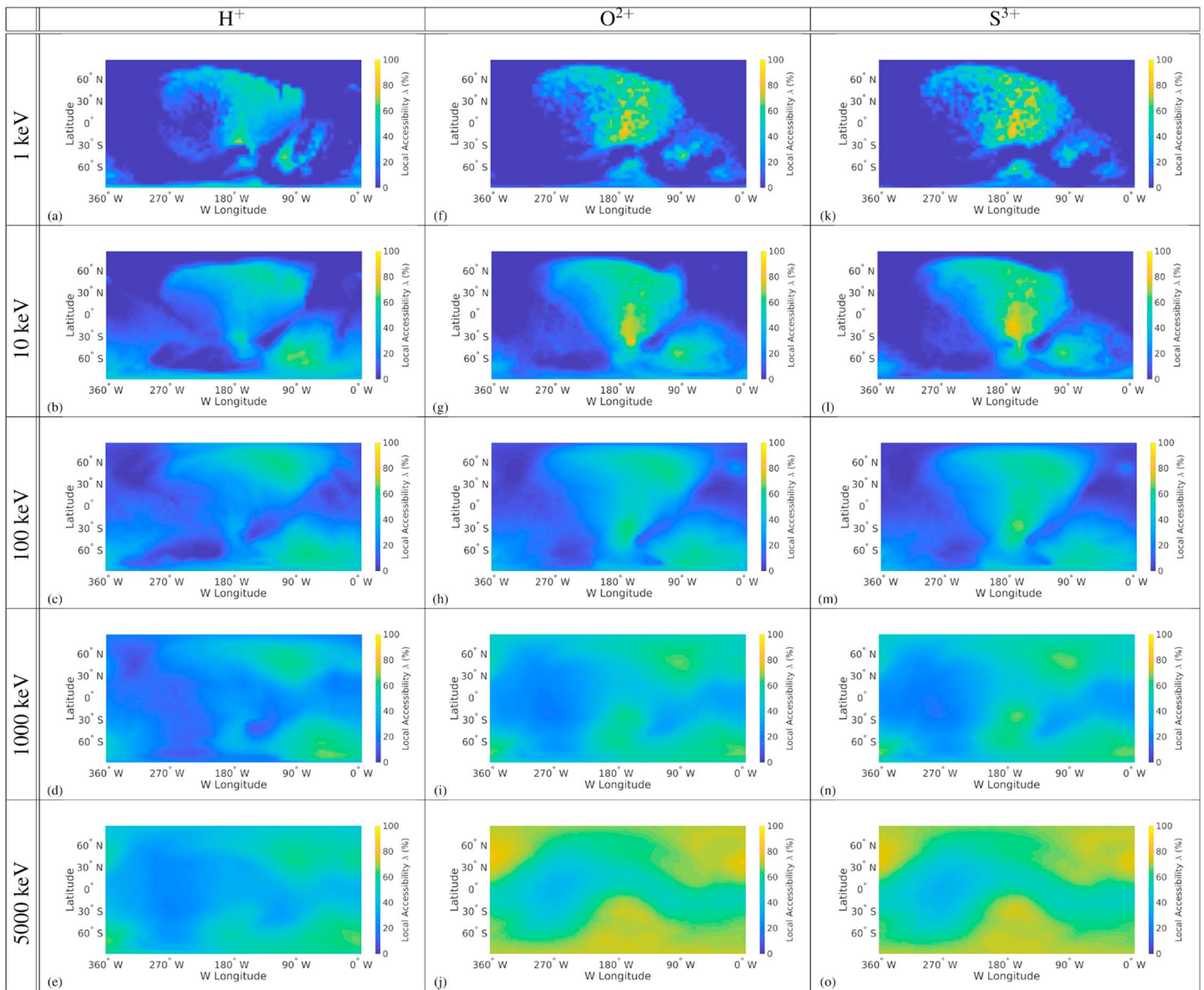


**Figure 5.** (a–o) Accessibility of Europa’s surface to energetic magnetospheric ions in Scenario # 3, which takes into account the field perturbations generated by the deflection of the thermal magnetospheric flow around the moon’s ionosphere and induced dipole.

Due to the inclusion of a south polar plume, Europa’s Alfvén wings are slightly asymmetric between both hemispheres. In particular, as can be seen from Figure 1a, the region of strongest field line draping in the southern wing (depicted in dark red) is slightly offset in ( $-z$ ) direction; that is, it is located farther away from Europa’s surface than in the northern hemisphere. Such a displacement of the southern wing has actually been identified in Cassini magnetic field observations from flybys through the Enceladus plume (e.g., Dougherty et al., 2006; Kriegel et al., 2011). However, due to the much larger extension of the Enceladus plume (compared to the size of the moon itself), the displacement there is on the order of one Enceladus radius. The subtle north-south asymmetry in Europa’s Alfvén wings has a weak but discernible influence on the ion accessibility patterns at polar latitudes. As can be seen in the first two rows of Figure 5, the value of  $\lambda$  for 1- to 10-keV ions drops to nearly 0 at Europa’s north pole, whereas a value on the order of  $\lambda \approx 30 - 40\%$  is achieved in parts of the south polar cap. In the northern hemisphere, the strong field line draping close to the surface facilitates the impact of gyrating ions shortly after launch. However, the slight offset of the most intense draping in the southern wing allows a larger fraction of ions to travel away from Europa along field lines locally perpendicular to the surface. The resulting increase in  $\lambda$  (compared to the north) is rather

subtle and completely disappears at initial ion energies around 100 keV (bottom three rows of Figure 5). We note that a similar effect of the draped fields on energetic ion dynamics has been identified at Saturn's moon Titan; see discussion of Figure 8 in Kabanovic et al. (2018).

In the model setup considered here, the “visibility” of the plume in the accessibility maps is also attenuated by the fact that the Alfvén wing characteristics are inclined against the  $(x, z)$  plane by about  $\arctan(210/450) = 25^\circ$ ; that is, the transverse currents in the plume do not feed directly into the core region of the southern Alfvénic fluxtube. The influence of local atmospheric inhomogeneities on energetic ion accessibility will be investigated in more detail in section 3.4 where we consider a fully realistic flyby scenario.

Overall, comparing the accessibility maps from Scenarios # 2 and # 3 strongly suggests that the field perturbations generated by Europa's thermal plasma interaction need to be taken into account by any reasonable model of energetic ion precipitation onto the moon. This is indeed expected, since—despite their energies in the kiloelectron volt/megaelectron volt range—the gyroradii of the energetic ions are still small, compared to the length scales of Europa's Alfvénic plasma interaction and to the diameter of the moon itself. This aspect is a major difference to energetic ion dynamics at Callisto, where—in the megaelectron volt regime—the ions can evade deflection in the perturbed fields by gyrating around the Alfvén wings.

### 3.4. Scenarios # 4 and # 5: Energetic Ion Precipitation During the Galileo E26 Flyby

Finally, we analyze the precipitation of energetic ions onto Europa for a fully realistic interaction scenario. More specifically, we consider Europa's interaction with its magnetospheric environment, as observed during the Galileo E26 flyby on 3 January 2000. For this encounter, Arnold et al. (2019) modeled the moon's electromagnetic environment with (Scenario # 4) and without (Scenario # 5) a water vapor plume in the southern trailing hemisphere (longitude  $300^\circ\text{W}$ , latitude  $50^\circ\text{S}$ ) and achieved excellent quantitative agreement with Galileo magnetic field observations. The corresponding accessibility maps are displayed in Figures 6 (Scenario # 4, plume included) and 7 (Scenario # 5, no plume). In addition, we present a three-dimensional illustration of 10-keV oxygen ion accessibility for both scenarios in Figure 8. All specifics of the hybrid code setup mentioned in the following are discussed in detail by Arnold et al. (2019).

Compared to Scenario # 3, the complexity of the E26 setup is again increased: (i) The ram-wake asymmetry of Europa's global atmosphere is taken into account. The neutral gas density at the moon's ramside apex is an order of magnitude larger than at its wakeside apex. (ii) The axis of the water vapor plume in Scenario # 4 is no longer parallel to the local surface normal direction nor is aligned with any axis of the EPhiO system. (iii) While the observed magnetospheric background field  $\underline{B}_0 = (-22, 205, -379)$  nT is only slightly weaker than in the preceding cases ( $|\underline{B}_0| = 431$  nT), the field now possesses three nonzero components. Thus, even if the induced dipole were absent and the density profile of Europa's global atmosphere were isotropic, the magnetic draping pattern and the Alfvén wings would no longer be symmetric with respect to any plane that contains the  $x$  axis (e.g., Simon & Motschmann, 2009).

Figures 6–8 reveal a completely different picture than the model setups without plasma currents, again emphasizing the tremendous influence of the electromagnetic field perturbations on energetic ion dynamics near Europa. As can be seen in Figures 6a, 6f, and 6k, at initial energies of 1-keV large portions of Europa's surface are nearly inaccessible to precipitating ions, similar to Scenario # 3. The most notable region of nonzero accessibility is a “patch” centered in the moon's southern, Jupiter-averted hemisphere. This patch is also close to the region where the plume generates multiple fine structures in the magnetic field on scales of only  $0.1R_E$  (see Figure 3 in Arnold et al., 2019). However, the plume source itself, located at a longitude of  $300^\circ\text{W}$  and a southern latitude of  $50^\circ$ , does not have a discernible influence on the accessibility of 1- to 10-keV ions in its immediate vicinity: a comparison of the first rows in Figures 6 and 7 illustrates that  $\lambda$  is nearly zero around that location in both cases.

Most strikingly, at all initial energies  $E \leq 100$  keV Europa's thermal plasma interaction during E26 provided extremely efficient shielding of the surface against energetic ion impacts: From large segments of the surface, backtraced ions can not escape at all, and in less than 10% of the surface area, the value of  $\lambda$  exceeds 90% (see also Figure 8). At initial ion energies of  $E \geq 1,000$  keV, the accessibility pattern (fourth and fifth rows of Figures 6 and 7) again begins to exhibit some similarity to the results of Scenario # 2. However, only at energies of  $E \approx 5,000$  keV does the accessibility pattern display the characteristic wavy depletion region at equatorial latitudes (see bottom row of Figure 3) that is associated with the uniform background field alone.

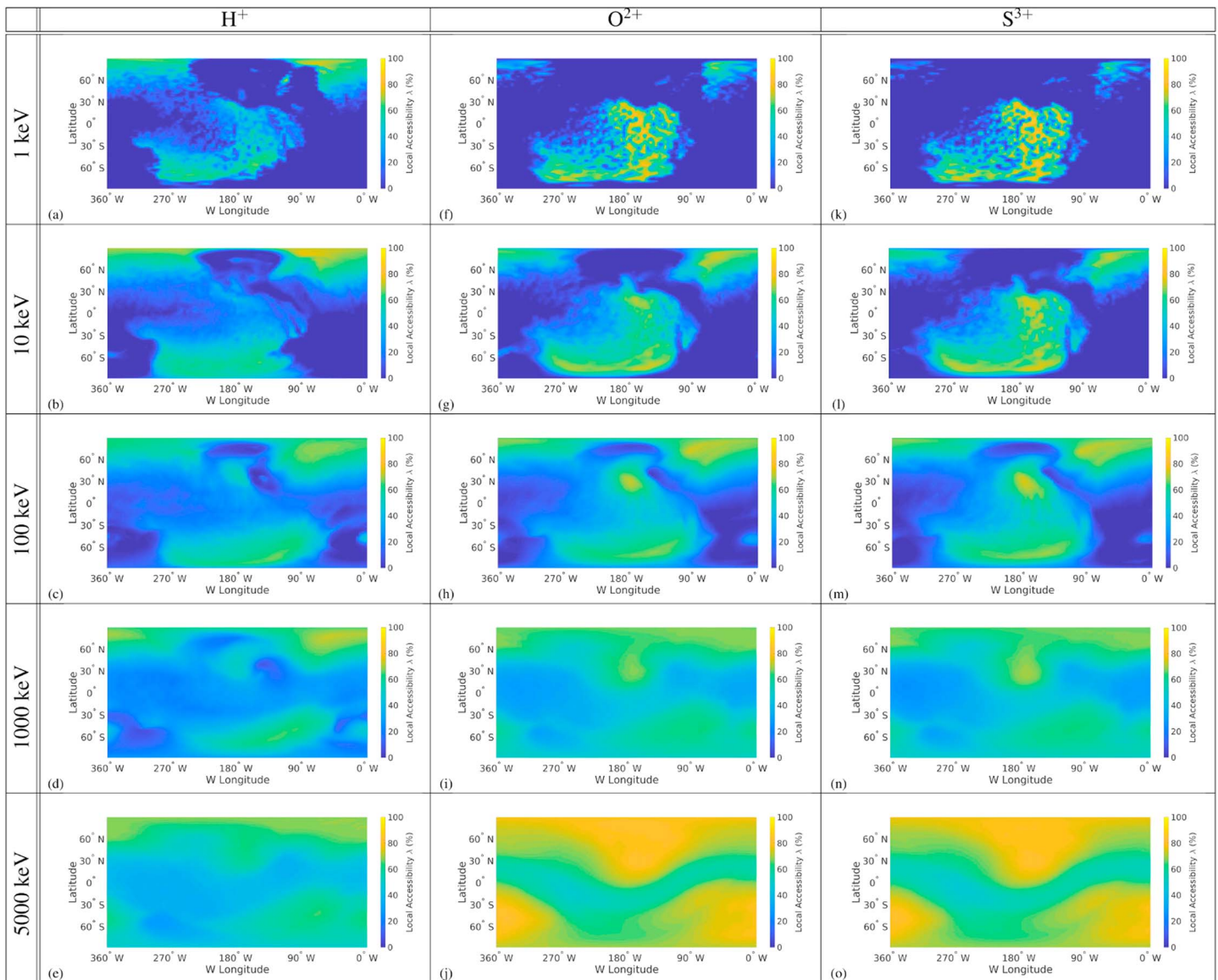


**Figure 6.** (a–o) Maps of Europa’s surface accessibility to energetic magnetospheric ions during the Galileo E26 flyby (Scenario # 4). At the time of this encounter, Jupiter’s magnetospheric plasma interacted with Europa’s induced dipole field and global atmosphere as well as a local plume source in the moon’s southern trailing hemisphere. The electromagnetic fields have been taken from Run 1 of Arnold et al. (2019).

Thus, the influence of plasma interaction currents on the precipitation patterns can be neglected above these energies. Scenario # 2 still revealed a minor contribution of the induced dipole to the accessibility patterns in the megaelectron volt regime: The dipole confined regions of reduced  $\lambda$  close to equatorial latitudes; that is, the patterns appeared less wavy than in Figures 6 and 7. The weaker magnetospheric field during E26 (compared to Scenario #2) goes along with slightly larger ion gyroradii, which may partially explain this discrepancy. However, the complex setup of the E26 model does not allow to further constrain the contribution of the induced field at megaelectron volt energies.

A comparison between Figures 6 and 7 at any energy illustrates that, while inclusion of the plume source has only weak influence on the overall shape of the accessibility patterns, it does generate discernible changes in the values of  $\lambda$ , even at large distances to the atmospheric inhomogeneity. Most notably, in Scenario # 5 the patch of elevated accessibility features more extended regions with  $\lambda \geq 80\%$  near the equator than in Scenario # 4. Figure 2 of Arnold et al. (2019) shows that inclusion of the plume generates a local decrease in the intensity of the  $B_x$  perturbations; that is, the field lines near equatorial latitudes become more aligned with the background field direction (similar to Scenario # 2). As discussed in section 3.2, this facilitates

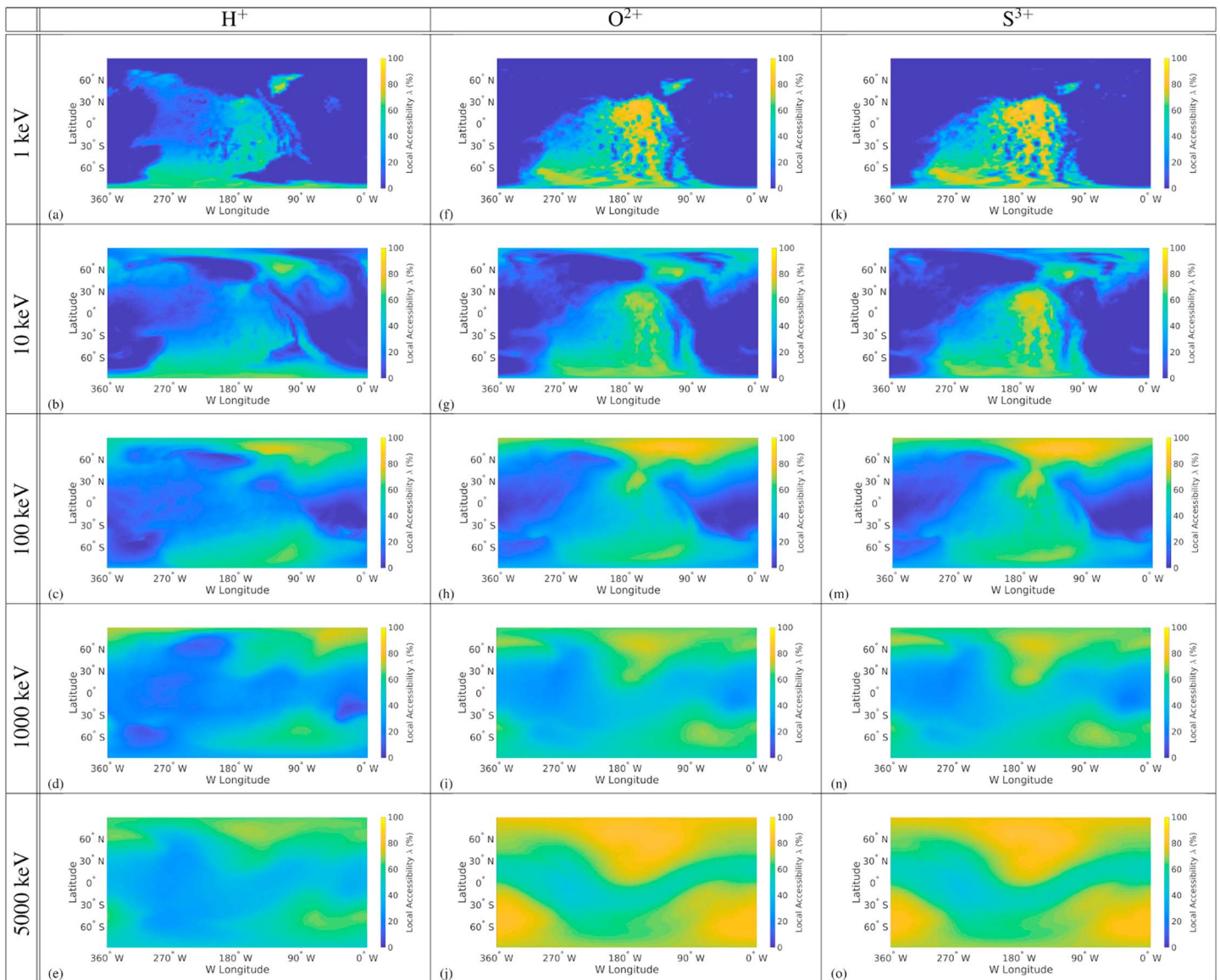


**Figure 7.** (a–o) Energetic ion accessibility during Galileo flyby E26 (Scenario # 5). The hybrid model included the same upstream parameters, induced dipole moment and global atmosphere as Scenario # 4 (see Figure 6). However, for the results shown here, the plume of water vapor in Europa's southern trailing hemisphere has been removed from the hybrid simulation. The AIKEF setup corresponds to Run 5 in Arnold et al. (2019).

the impact of backtraced ions launched near the equator. These results also emphasize that, due to the translational invariance of the Alfvén wings (Neubauer, 1980), inclusion of the plume does not only have local influence on energetic ion dynamics: The modified current systems in the wings may intercept and deflect approaching ions even at large distances to Europa.

The accessibility patterns calculated for the E26 flyby (Scenarios # 4 and # 5) display substantial differences to the  $\lambda$  maps obtained for Callisto in a (qualitatively) similar electromagnetic field configuration. Liuzzo et al. (2019) analyzed the accessibility of Callisto's surface to energetic ions during the Galileo C3, C9, and C10 flybys (see Figure 13 in that work). During the first two flybys, Callisto was located far above (C3) or below (C9) the center of Jupiter's magnetospheric current sheet; that is, plasma interaction currents were weak and the  $\lambda$  maps from these two flybys are best compared to Scenario # 2 in the present study. However, during the C10 flyby Callisto was located closer to the center of the Jovian current sheet, and the thermal plasma interaction (e.g., draping and pileup) made substantial contributions to the fields near the moon. As shown by Liuzzo et al. (2019), even at initial ion energies of up to  $E = 1$  MeV, the induced dipole at Callisto during C10 generated characteristic clusters of high accessibility near the moon's magnetic poles. However,

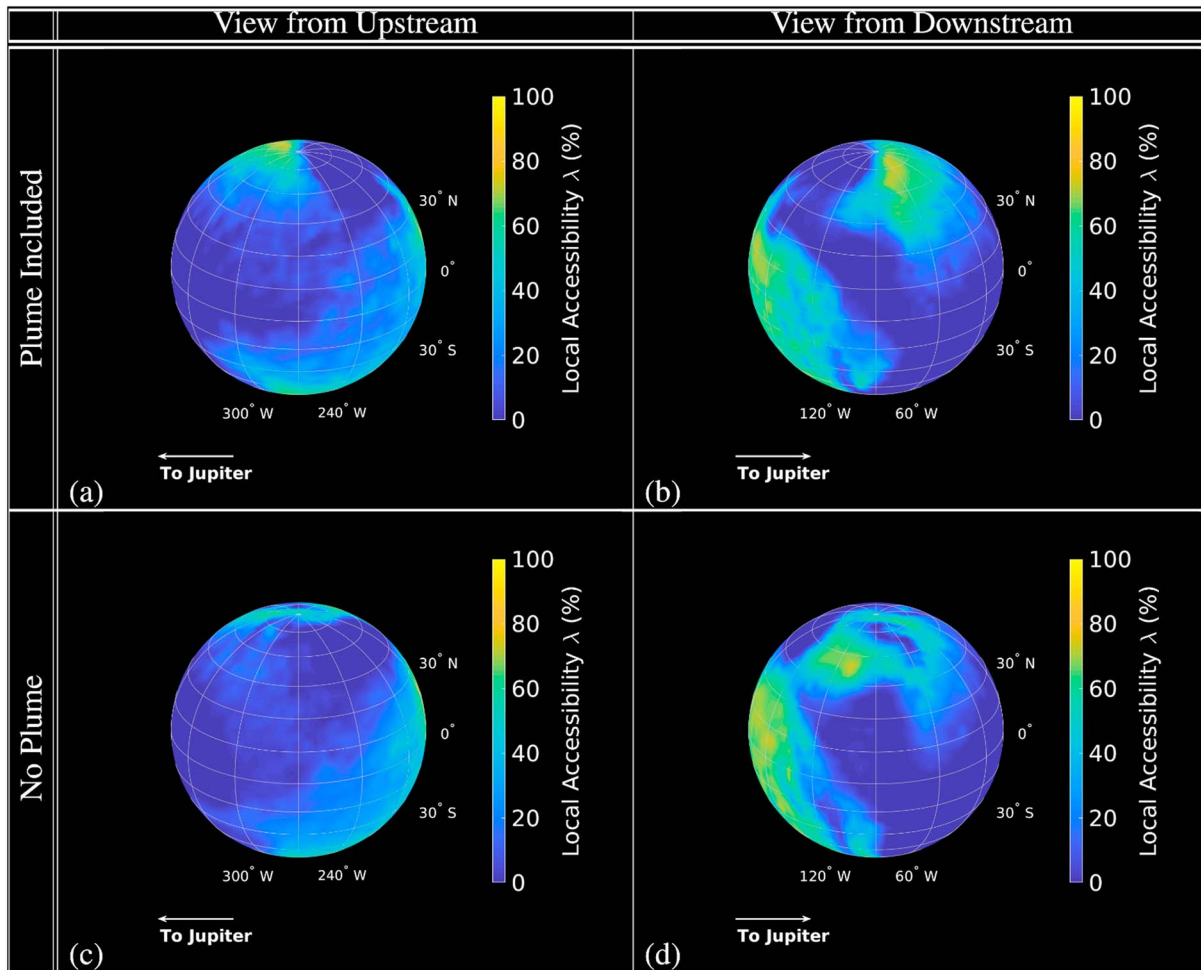


**Figure 8.** Comparison of the accessibility maps for 10-keV oxygen ions during the E26 flyby: (a, b) For Scenario # 4, that is, with the plume included, and (c, d) for Scenario # 5, that is, without the plume. The accessibility maps shown here are the same as in Figures 6g and 7g, projected onto the moon's surface. In (a) and (c), the vantage point is located upstream of Europa and slightly offset toward the northern hemisphere. In (b) and (d), the vantage point is located at the moon's wakeside.

due to the diminished contribution of the induced dipole to the total field at Europa (see section 3.2), these clusters do not appear at all in our results from Scenarios # 4 and # 5. Also, ion gyration around Callisto already made the C10 accessibility patterns become quasi-homogeneous at an initial energy of  $E = 5$  MeV (see Figure 13o in Liuzzo et al., 2019). At Europa, this homogenization occurs at much higher energies, since at a given initial value of  $E$ , ion gyroradii are an entire order of magnitude smaller than at Callisto.

During E26, the energetic ion distribution  $I_0(E)$  outside of Europa's interaction region has been measured by Galileo's EPD; see Figure 4 in Paranicas et al. (2009). To further investigate the attenuation of the energetic ion flux in Europa's perturbed electromagnetic environment, we have applied the GENTOO output to estimate the ion distribution  $I(E)$  at different locations on Europa's surface. As discussed by Regoli et al. (2016) for Titan and Liuzzo et al. (2019) for Callisto, these two quantities are related through  $I(E) = \lambda(E)I_0(E)$ , with the energy-dependent accessibility  $\lambda(E)$  at the respective surface location. In agreement with Mauk et al. (2004), this expression assumes the pitch angle distribution of energetic ions outside of Europa's interaction region to be isotropic. Also, it is assumed that the ions' gain/loss in energy when traveling through the perturbed fields within the AIKEF domain remains well below the initial energy of the ions. In the 10-keV to 10-MeV regime, this assumption is well fulfilled at Europa. For instance, the lowest-energy channel of the EPD instrument measured particles in the range from 22 to 42 keV (Williams et al., 1992). When exposed to the  $\vec{E} \times \vec{B}$  drift, the gain in energy for a 22-keV oxygen ion is on the order of 9 keV; that is, the difference to the initial energy cannot be resolved by the relevant EPD channel. In the "worst case," an ion would be displaced to higher energies by a single channel.

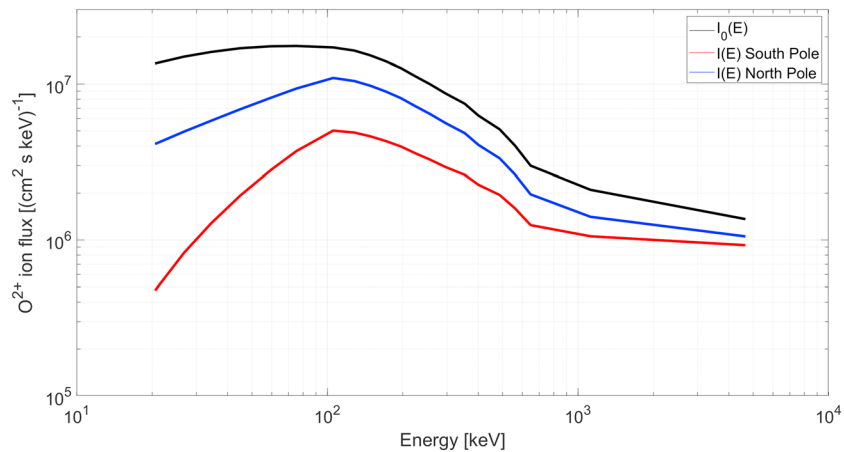


**Figure 9.** Intensity of the energetic oxygen ion flux near Europa during the Galileo E26 flyby on 3 January 2000. The black line represents the ion flux measured outside of Europa's plasma interaction region by the Galileo Energetic Particles Detector instrument, as provided in Figure 4 of Paranicas et al. (2009). The blue and red lines show the energetic oxygen flux at Europa's north and south poles, respectively, as obtained from the GENTOO model. At energies in the kiloelectron volt regime, the shielding effect caused by Europa's thermal plasma interaction decreases the incident particle flux by more than an order of magnitude.

The modified energy spectrograms calculated in this way are displayed in Figure 9 for Europa's south pole (red) and north pole (blue). As can be seen, the shielding of Europa's surface by the draped fields reduces the incident particle flux by up to a factor of  $\approx 20$ . Also, the field perturbations near Europa are asymmetric between the northern and southern hemispheres (mainly due to the inclined magnetospheric background field). Below energies of 1 MeV, the resulting hemispherical disparities in the draping pattern generate differences between the energetic ion influx at Europa's north and south poles by up to an entire order of magnitude (see Figure 9). Consistent with our accessibility maps, above 1 MeV the energy spectra modeled for Europa's poles start to converge against each other and also come closer to the  $I_0(E)$  measured outside of the moon's interaction region.

In general, two important lessons are to be learned from Scenarios # 4 and # 5: (i) Due to its effect on the current systems and fields at remote locations (e.g., Blöcker et al., 2016), a local atmospheric inhomogeneity may affect the ion accessibility pattern even at distant points on Europa's surface. (ii) However, the influence of such an inhomogeneity on the precipitation pattern of energetic ions is rather subtle and mostly quantitative in nature (as also seen in Europa's polar regions for Scenario # 3).

#### 4. Summary and Concluding Remarks

In this study, we have combined the electromagnetic field output from a hybrid model (Arnold et al., 2019) with a backtracing tool for energetic particles (Liuzzo et al., 2019) to analyze the accessibility of Europa's surface to energetic magnetospheric hydrogen, oxygen, and sulfur ions. While all preceding studies of energetic ion dynamics assume the electromagnetic fields near Europa to be spatially uniform, we have systematically investigated the contributions of the moon's induced dipole field and draping of the magnetospheric field to the resulting ion precipitation patterns. We demonstrated that the induced dipole alone mainly generates quantitative changes in the accessibility patterns, confining regions of reduced accessibility to a narrow belt around Europa's equator. However, the field perturbations generated by Europa's thermal plasma interaction (mass loading and flow deflection around the induced dipole) cause a drastic drop in the overall accessibility of the moon's surface to energetic ions, especially for particle energies below 1 MeV. When Europa's thermal plasma interaction is taken into account, energetic ion precipitation is confined to characteristic patches on the surface, the locations and size of which are determined by the thermal upstream plasma conditions and the components included to represent the Europa obstacle (e.g., the complexity of the atmosphere model). Throughout all scenarios considered, we find that Europa's polar regions display the highest accessibilities for protons in the megaelectron volt regime and heavy ions. Regardless of ion species and energy, the precipitation patterns at equatorial latitudes depend much stronger on the chosen setup for the electromagnetic fields. In any case, our results clearly illustrate that the electromagnetic field perturbations

caused by Europa's thermal plasma interaction need to be taken into account to obtain a realistic picture of surface precipitation for a specific set of upstream conditions.

The results of Scenarios # 3 to # 5 suggest that at energies of  $E = 10$  keV and lower, the bulk of the magnetospheric plasma is diverted around Europa by the draped electromagnetic fields. In consequence, this low-energy magnetospheric plasma is unlikely to make significant contributions to the erosion of Europa's surface and therefore to the generation of its dilute gas envelope. Only in highly localized "patchy" regions, the surface accessibility for  $E \leq 10$  keV is above  $\lambda \approx 50\%$ , and therefore, the surface can be eroded by magnetospheric plasma from this energy regime. The patchy regions that can potentially be sputtered move across the surface in synchronism with the changes of Europa's electromagnetic environment when Jupiter's magnetospheric current sheet sweeps over the moon. Our results also suggest that in the upper kiloelectron volt and the megaelectron volt regime, Europa's polar caps are exposed to (more or less) continuous precipitation by heavy ions, thereby allowing these regions to serve as a persistent source of exospheric particles. The detailed physics of surface erosion depends on various parameters, such as the material and temperature of the surface (e.g., Spencer et al., 1999), that will be taken into account in a follow-up study.

When considering time scales of multiple Jovian rotations, the question arises whether the change in surface accessibility caused by the thermal plasma currents would average out, moving the resulting precipitation and surface sputtering patterns closer to those in Cassidy et al. (2013). Addressing this question will require to systematically model Europa's thermal plasma environment at Numerous System III longitudes and—taking into account the local time asymmetries of the moon's global atmosphere (Plainaki et al., 2013)—also at different angles of the incident solar flux against the corotation direction. This effort is beyond the scope of the present study. However, in contrast to Callisto, the thermal plasma interaction makes significant contributions to Europa's magnetic environment even at large distances to the center of Jupiter's magnetospheric current sheet (e.g., Arnold et al., 2019; Zimmer et al., 2000). Thus, the protective "shield" rendered by the draped fields and the resulting drop in energetic ion precipitation will always be present, with its strength being weakest (but still nonnegligible) at large distances to the sheet and strongest near its center.

Systematically modeling the evolution of energetic ion precipitation onto Europa will also be necessary to explain, for example, the patterns of hydrated sulfuric acid observed on the moon's surface by Galileo (e.g., Carlson et al., 2005). At first glance, the patterns observed in Europa's trailing hemisphere are not consistent with the sulfur precipitation maps from any of the *individual* field configurations considered in our study. This issue can probably be addressed by averaging the precipitating particle fluxes at specific surface locations over a full period of Jupiter's current sheet oscillation around Europa's orbital plane.

## References

- Arnold, H., Liuzzo, L., & Simon, S. (2019). Magnetic signatures of a plume at Europa during the Galileo E26 flyby. *Geophysical Research Letters*, *46*, 1149–1157. <https://doi.org/10.1029/2018GL081544>
- Blöcker, A., Saur, J., & Roth, L. (2016). Europa's plasma interaction with an inhomogeneous atmosphere: Development of Alfvén winglets within the Alfvén wings. *Journal of Geophysical Research: Space Physics*, *121*, 9794–9828. <https://doi.org/10.1002/2016JA022479>
- Carlson, R. W., Anderson, M. S., Mehlman, R., & Johnson, R. E. (2005). Distribution of hydrate on Europa: Further evidence for sulfuric acid hydrate. *Icarus*, *177*, 461–471. <https://doi.org/10.1016/j.icarus.2005.03.026>
- Cassidy, T. A., Paranicas, C. P., Shirley, J. H., Dalton, J. B. III, Teolis, B. D., Johnson, R. E., & Hendrix, A. R. (2013). Magnetospheric ion sputtering and water ice grain size at Europa. *Planetary and Space Science*, *77*, 64–73. <https://doi.org/10.1016/j.pss.2012.07.008>
- Clark, G., Mauk, B. H., Paranicas, C., Kollmann, P., & Smith, H. T. (2016). Charge states of energetic oxygen and sulfur ions in Jupiter's magnetosphere. *Journal of Geophysical Research: Space Physics*, *121*, 2264–2273. <https://doi.org/10.1002/2015JA022257>
- Collier, M. R., & Hamilton, D. (1995). The relationship between kappa and temperature in energetic ion spectra at Jupiter. *Geophysical Research Letters*, *22*(3), 303–306. <https://doi.org/10.1029/94GL02997>
- Cooper, J. F., Johnson, R. E., Mauk, B. H., Garrett, H. B., & Gehrels, N. (2001). Energetic ion and electron irradiation of the icy Galilean satellites. *Icarus*, *149*(1), 133–159. <https://doi.org/10.1006/icar.2000.6498>
- Dougherty, M. K., Khurana, K. K., Neubauer, F. M., Russell, C. T., Saur, J., Leisner, J. S., & Burton, M. E. (2006). Identification of a dynamic atmosphere at Enceladus with the Cassini magnetometer. *Science*, *311*(5766), 1406–1409. <https://doi.org/10.1126/science.1120985>
- Fatemi, S., Poppe, A., Khurana, K., Holmström, M., & Delory, G. (2016). On the formation of Ganymede's surface brightness asymmetries: Kinetic simulations of Ganymede's magnetosphere. *Geophysical Research Letters*, *10*, 4745–4754. <https://doi.org/10.1002/2016GL068363>
- Feyerabend, M., Simon, S., Motschmann, U., & Liuzzo, L. (2015). Filamented ion tail structures at Titan: A hybrid simulation study. *Planetary and Space Science*, *117*, 362–376. <https://doi.org/10.1016/j.pss.2015.07.008>
- Feyerabend, M., Simon, S., Neubauer, F. M., Motschmann, U., Bertucci, C., Edberg, N. J. T., & Kurth, W. S. (2016). Hybrid simulation of Titan's interaction with the supersonic solar wind during Cassini's T96 flyby. *Geophysical Research Letters*, *43*, 35–42. <https://doi.org/10.1002/2015GL066848>

## Acknowledgments

**Funding sources:** The authors are grateful to the National Aeronautics and Space Administration (NASA) for financial support through the *Solar System Workings 2016* program, Grant 80NSSC17K0772. In addition, the work of Benjamin Breer and Peter Andersson was supported by the Georgia Tech *President's Undergraduate Research Award (PURA)*. Our research was supported in part through research cyberinfrastructure resources and services provided by the *Partnership for an Advanced Computing Environment (PACE)* at the Georgia Institute of Technology.

**Author contributions:** Benjamin Breer carried out the energetic particle tracing simulations with the GENTOO code, visualized, and analyzed the results. Peter Andersson assisted with the GENTOO simulations. Lucas Liuzzo developed the original GENTOO code for Callisto and advised Benjamin Breer and Peter Andersson in its application to Europa. Hannes Arnold developed the AIKEF hybrid model for Europa and generated the three-dimensional data cubes of the electromagnetic fields. Sven Simon and Lucas Liuzzo wrote the manuscript with the help of the other coauthors. Sven Simon is also the principal investigator of NASA Project 80NSSC17K0772.

**Data availability:** The data used to generate the figures presented in this manuscript can be downloaded from the website (<https://zenodo.org/record/3385296#.XW8OI3pCUk>) or, alternatively, from the Zenodo (<https://doi.org/10.5281/zenodo.3385295>).

The authors would like to thank Chris Paranicas and another referee for careful inspection of the manuscript and for valuable comments.

- Ip, W. H., Williams, D., McEntire, R., & Mauk, B. (1998). Ion sputtering and surface erosion at Europa. *Geophysical Research Letters*, *25*(6), 829–832. <https://doi.org/10.1029/98GL00472>
- Jia, X., Kivelson, M. G., Khurana, K. K., & Kurth, W. S. (2018). Evidence of a plume on Europa from Galileo magnetic and plasma wave signatures. *Nature Astronomy*, *2*, 459–464. <https://doi.org/10.1038/s41550-018-0450-z>
- Johnson, R. E., Burger, M. H., Cassidy, T. A., Leblanc, F., Marconi, M., & Smyth, W. H. (2009). Composition and detection of Europa's sputter-induced atmosphere. In R. T. Pappalardo, W. B. McKinnon, & K. K. Khurana (Eds.), *Europa* (pp. 507). Tucson: University of Arizona Press.
- Kabanovic, S., Feyerabend, M., Simon, S., Meeks, Z., & Wulms, V. (2018). Influence of asymmetries in the magnetic draping pattern at Titan on the emission of energetic neutral atoms. *Planetary and Space Science*, *152*, 142–164. <https://doi.org/10.1016/j.pss.2017.12.017>
- Kabin, K., Combi, M. R., Gombosi, T. I., Nagy, A. F., DeZeeuw, D. L., & Powell, K. G. (1999). On Europa's magnetospheric interaction: A MHD simulation of the E4 flyby. *Journal of Geophysical Research*, *104*(A9), 19,983–19,992. <https://doi.org/10.1029/1999JA900263>
- Keppeler, E., & Krupp, N. (1996). The charge state of helium in the Jovian magnetosphere: A possible method to determine it. *Planetary and Space Science*, *44*(2), 71–75. [https://doi.org/10.1016/0032-0633\(95\)00076-3](https://doi.org/10.1016/0032-0633(95)00076-3)
- Khurana, K. K., Kivelson, M. G., Stevenson, D. J., Schubert, G., Russell, C. T., Walker, R. J., & Polansky, C. (1998). Induced magnetic fields as evidence for subsurface oceans in Europa and Callisto. *Nature*, *395*(6704), 777–780. <https://doi.org/10.1038/27394>
- Kivelson, M. G., Bagenal, F., Kurth, W. S., Neubauer, F. M., Paranicas, C., & Saur, J. (2004). Magnetospheric interactions with satellites. In F. Bagenal, T. E. Dowling, & W. B. McKinnon (Eds.), *Jupiter. The planet, satellites and magnetosphere* (pp. 513–536). Cambridge: Cambridge University Press.
- Kivelson, M. G., Khurana, K. K., Stevenson, D. J., Bennett, L., Joy, S., Russell, C. T., & Polansky, C. (1999). Europa and Callisto: Induced or intrinsic fields in a periodically varying plasma environment. *Journal of Geophysical Research*, *104*(A3), 4609–4626. <https://doi.org/10.1029/1998JA900095>
- Kivelson, M. G., Khurana, K. K., & Volwerk, M. (2009). Europa's interaction with the Jovian magnetosphere. In R. T. Pappalardo, W. B. McKinnon, & K. K. Khurana (Eds.), *Europa* (pp. 545). Tucson: University of Arizona Press.
- Kotova, A., Roussos, E., Krupp, N., & Dandouras, I. (2015). Modeling of the energetic ion observations in the vicinity of Rhea and Dione. *Icarus*, *258*, 402–417. <https://doi.org/10.1016/j.icarus.2015.06.031>
- Kriegel, H., Simon, S., Meier, P., Motschmann, U., Saur, J., Wennmacher, A., & Dougherty, M. K. (2014). Ion densities and magnetic signatures of dust pick-up at Enceladus. *Journal of Geophysical Research: Space Physics*, *119*, 2740–2774. <https://doi.org/10.1002/2013JA019440>
- Kriegel, H., Simon, S., Motschmann, U., Saur, J., Neubauer, F. M., Persoon, A. M., & Gurnett, D. A. (2011). Influence of negatively charged plume grains on the structure of Enceladus' Alfvén wings: Hybrid simulations versus Cassini MAG data. *Journal of Geophysical Research*, *116*, A10223. <https://doi.org/10.1029/2011JA016842>
- Kriegel, H., Simon, S., Müller, J., Motschmann, U., Saur, J., Glassmeier, K., & Dougherty, M. K. (2009). The plasma interaction of Enceladus: 3D hybrid simulations and comparison with Cassini MAG data. *Planetary and Space Science*, *57*(14–15), 2113–2122. <https://doi.org/10.1016/j.pss.2009.09.025>
- Krupp, N., Roussos, E., Kriegel, H., Kollmann, P., Kivelson, M. G., Kotova, A., & Khurana, K. K. (2013). Energetic particle measurements in the vicinity of Dione during the three Cassini encounters 2005–2011. *Icarus*, *226*(1), 617–628. <https://doi.org/10.1016/j.icarus.2013.06.007>
- Liuzzo, L., Feyerabend, M., Simon, S., & Motschmann, U. (2015). The impact of Callisto's atmosphere on its plasma interaction with the Jovian magnetosphere. *Journal of Geophysical Research: Space Physics*, *120*, 9401–9427. <https://doi.org/10.1002/2015JA021792>
- Liuzzo, L., Simon, S., & Feyerabend, M. (2018). Observability of Callisto's inductive signature during the JUPITER ICy moons Explorer mission. *Journal of Geophysical Research: Space Physics*, *123*, 9045–9054. <https://doi.org/10.1002/2018JA025951>
- Liuzzo, L., Simon, S., Feyerabend, M., & Motschmann, U. (2016). Disentangling plasma interaction and induction signatures at Callisto: The Galileo C10 flyby. *Journal of Geophysical Research: Space Physics*, *121*, 8677–8694. <https://doi.org/10.1002/2016JA023236>
- Liuzzo, L., Simon, S., Feyerabend, M., & Motschmann, U. (2017). Magnetic signatures of plasma interaction and induction at Callisto: The Galileo C21, C22, C23, and C30 flybys. *Journal of Geophysical Research: Space Physics*, *122*, 7364–7386. <https://doi.org/10.1002/2017JA024303>
- Liuzzo, L., Simon, S., & Regoli, L. (2019). Energetic ion dynamics near Callisto. *Planetary and Space Science*, *166*, 23–53. <https://doi.org/10.1016/j.pss.2018.07.014>
- Mauk, B., Mitchell, D., McEntire, R., Paranicas, C., Roelof, E., Williams, D., & Lagg, A. (2004). Energetic ion characteristics and neutral gas interactions in Jupiter's magnetosphere. *Journal of Geophysical Research*, *109*, A09S12. <https://doi.org/10.1029/2003JA010270>
- McGrath, M. A., Hansen, C. J., & Hendrix, A. R. (2009). Observations of Europa's tenuous atmosphere. In R. T. Pappalardo, W. B. McKinnon, & K. K. Khurana (Eds.), *Europa* (pp. 485). Tucson: University of Arizona Press.
- Müller, J., Simon, S., Motschmann, U., Schüle, J., Glassmeier, K., & Pringle, G. J. (2011). A.I.K.E.F.: Adaptive hybrid model for space plasma simulations. *Computer Physics Communications*, *182*(4), 946–966. <https://doi.org/10.1016/j.cpc.2010.12.033>
- Nénon, Q., & André, N. (2019). Evidence of Europa neutral gas torii from energetic sulfur ion measurements. *Geophysical Research Letters*, *46*, 3599–3606. <https://doi.org/10.1029/2019GL082200>
- Neubauer, F. M. (1980). Nonlinear standing Alfvén wave current system at Io—Theory. *Journal of Geophysical Research*, *85*, 1171–1178. <https://doi.org/10.1029/JA085iA03p01171>
- Neubauer, F. M. (1998). The sub-Alfvénic interaction of the Galilean satellites with the Jovian magnetosphere. *Journal of Geophysical Research*, *103*, 19,843–19,866. <https://doi.org/10.1029/97JE03370>
- Neubauer, F. M. (1999). Alfvén wings and electromagnetic induction in the interiors: Europa and Callisto. *Journal of Geophysical Research*, *104*, 28,671–28,684. <https://doi.org/10.1029/1999JA900217>
- Nordheim, T. A., Hand, K. P., & Paranicas, C. (2018). Preservation of potential biosignatures in the shallow subsurface of Europa. *Nature Astronomy*, *2*, 673–679. <https://doi.org/10.1038/s41550-018-0499-8>
- Paranicas, C., Carlson, R., & Johnson, R. (2001). Electron bombardment of Europa. *Geophysical Research Letters*, *28*(4), 673–676. <https://doi.org/10.1029/2000GL012320>
- Paranicas, C., Cooper, J. F., Garrett, H. B., Johnson, R. E., & Sturmer, S. J. (2009). Europa's radiation environment and its effects on the surface. In R. T. Pappalardo, W. B. McKinnon, & K. K. Khurana (Eds.), *Europa* (pp. 529). Tucson: University of Arizona Press.
- Paranicas, C., McEntire, R. W., Cheng, A. F., Lagg, A., & Williams, D. J. (2000). Energetic charged particles near Europa. *Journal of Geophysical Research*, *105*, 16,005–16,016. <https://doi.org/10.1029/1999JA000350>
- Paranicas, C., Ratliff, J., Mauk, B., Cohen, C., & Johnson, R. (2002). The ion environment near Europa and its role in surface energetics. *Geophysical Research Letters*, *29*(5), 1074. <https://doi.org/10.1029/2001GL014127>

- Plainaki, C., Cassidy, T. A., Shematovich, V. I., Milillo, A., Wurz, P., Vorburger, A., & Teolis, B. (2018). Towards a global unified model of Europa's tenuous atmosphere. *Space Science Reviews*, 214, 40. <https://doi.org/10.1007/s11214-018-0469-6>
- Plainaki, C., Milillo, A., Mura, A., Saur, J., Orsini, S., & Massetti, S. (2013). Exospheric O<sub>2</sub> densities at Europa during different orbital phases. *Planetary and Space Science*, 88, 42–52. <https://doi.org/10.1016/j.pss.2013.08.011>
- Poppe, A. R., Fatemi, S., & Khurana, K. K. (2018). Thermal and energetic ion dynamics in Ganymede's magnetosphere. *Journal of Geophysical Research: Space Physics*, 123, 4614–4637. <https://doi.org/10.1029/2018JA025312>
- Pospieszalska, M. K., & Johnson, R. E. (1989). Magnetospheric ion bombardment profiles of satellites—Europa and Dione. *Icarus*, 78, 1–13. [https://doi.org/10.1016/0019-1035\(89\)90065-1](https://doi.org/10.1016/0019-1035(89)90065-1)
- Regoli, L., Roussos, E., Feyerabend, M., Jones, G. H., Krupp, N., Coates, A. J., & Dougherty, M. (2016). Access of energetic particles to Titan's exobase: A study of Cassini's T9 flyby. *Planetary and Space Science*, 130, 40–53. <https://doi.org/10.1016/j.pss.2015.11.013>
- Roth, L., Saur, J., Retherford, K. D., Strobel, D. F., Feldman, P. D., McGrath, M. A., & Nimmo, F. (2014). Transient water vapor at Europa's south pole. *Science*, 343(6167), 171–174. <https://doi.org/10.1126/science.1247051>
- Roussos, E., Kollmann, P., Krupp, N., Paranicas, C., Krimigis, S., Mitchell, D., et al. (2012). Energetic electron observations of Rhea's magnetospheric interaction. *Icarus*, 221(1), 116–134. <https://doi.org/10.1016/j.icarus.2012.07.006>
- Rubin, M., Jia, X., Altwegg, K., Combi, M. R., Daldorff, L. K. S., Gombosi, T. I., & Wurz, P. (2015). Self-consistent multifluid MHD simulations of Europa's exospheric interaction with Jupiter's magnetosphere. *Journal of Geophysical Research: Space Physics*, 120, 3503–3524. <https://doi.org/10.1002/2015JA021149>
- Saur, J., Neubauer, F. M., & Glassmeier, K. H. (2010). Induced magnetic fields in solar system bodies. *Space Science Reviews*, 152(1–4), 391–421.
- Saur, J., Strobel, D. F., & Neubauer, F. M. (1998). Interaction of the Jovian magnetosphere with Europa: Constraints on the neutral atmosphere. *Journal of Geophysical Research*, 103, 19,947–19,962. <https://doi.org/10.1029/97JE03556>
- Schilling, N., Khurana, K. K., & Kivelson, M. G. (2004). Limits on an intrinsic dipole moment in Europa. *Journal of Geophysical Research*, 109, E05006. <https://doi.org/10.1029/2003JE002166>
- Selesnick, R. S., & Cohen, C. M. S. (2009). Charge states of energetic ions in Jupiter's radiation belt inferred from absorption microsignatures of Io. *Journal of Geophysical Research*, 114, A01207. <https://doi.org/10.1029/2008JA013722>
- Seufert, M., Saur, J., & Neubauer, F. M. (2011). Multi-frequency electromagnetic sounding of the Galilean moons. *Icarus*, 214(2), 477–494. <https://doi.org/10.1016/j.icarus.2011.03.017>
- Simon, S., Krieger, H., Saur, J., Wennmacher, A., Neubauer, F. M., Roussos, E., & Dougherty, M. K. (2012). Analysis of Cassini magnetic field observations over the poles of Rhea. *Journal of Geophysical Research*, 117, A07211. <https://doi.org/10.1029/2012JA017747>
- Simon, S., & Motschmann, U. (2009). Titan's induced magnetosphere under non-ideal upstream conditions: 3D multi-species hybrid simulations. *Planetary and Space Science*, 57(14–15), 2001–2015. <https://doi.org/10.1016/j.pss.2009.08.010>
- Sparks, W. B., Hand, K. P., McGrath, M. A., Bergeron, E., Cracraft, M., & Deustua, S. E. (2016). Probing for evidence of plumes on Europa with HST/STIS. *The Astrophysical Journal*, 829(2), 121.
- Spencer, J. R., Tamppari, L. K., Martin, T. Z., & Travis, L. D. (1999). Temperatures on Europa from Galileo photopolarimeter-radiometer: Nighttime thermal anomalies. *Science*, 284, 1514. <https://doi.org/10.1126/science.284.5419.1514>
- Spohn, T., & Schubert, G. (2003). Oceans in the icy Galilean satellites of Jupiter? *Icarus*, 161, 456–467. [https://doi.org/10.1016/S0019-1035\(02\)00048-9](https://doi.org/10.1016/S0019-1035(02)00048-9)
- Truscott, P., Heynderickx, D., Sicard-Piet, A., & Bourdarie, S. (2011). Simulation of the radiation environment near Europa using the Geant4-based PLANETOCOSMICS-J model. *IEEE Transactions on Nuclear Science*, 58(6), 2776–2784. <https://doi.org/10.1109/TNS.2011.2172818>
- Volwerk, M., Khurana, K., & Kivelson, M. (2007). Europa's Alfvén wing: Shrinkage and displacement influenced by an induced magnetic field. *Annales Geophysicae*, 25(4), 905–914. <https://doi.org/10.5194/angeo-25-905-2007>
- Williams, D., McEntire, R., Jaskulek, S., & Wilken, B. (1992). The Galileo Energetic Particles Detector. *Space Science Reviews*, 60(1), 385–412. <https://doi.org/10.1007/BF00216863>
- Zimmer, C., Khurana, K. K., & Kivelson, M. G. (2000). Subsurface oceans on Europa and Callisto: Constraints from Galileo magnetometer observations. *Icarus*, 147(2), 329–347. <https://doi.org/10.1006/icar.2000.6456>